

2019 • 2020

Faculteit Industriële ingenieurswetenschappen
master in de industriële wetenschappen: chemie

Masterthesis

Photocatalytic degradation of an organic pollutant (Rhodamine B) under visible light irradiation using a bismuth iodide oxide, iron(II,III) oxide and (reduced) graphene oxide photocatalyst

PROMOTOR :

Prof. dr. ir. Leen BRAEKEN

PROMOTOR :

prof. dr. Lien NGUYEN HONG

COPROMOTOR :

Prof. Duc HOA NGUYEN

Kenneth Put

Scriptie ingediend tot het behalen van de graad van master in de industriële wetenschappen: chemie

Gezamenlijke opleiding UHasselt en KU Leuven



2019 • 2020

Faculteit Industriële ingenieurswetenschappen
master in de industriële wetenschappen: chemie

Masterthesis

Photocatalytic degradation of an organic pollutant (Rhodamine B) under visible light irradiation using a bismuth iodide oxide, iron(II,III) oxide and (reduced) graphene oxide photocatalyst

PROMOTOR :

Prof. dr. ir. Leen BRAEKEN

PROMOTOR :

prof. dr. Lien NGUYEN HONG

COPROMOTOR :

Prof. Duc HOA NGUYEN

Kenneth Put

Scriptie ingediend tot het behalen van de graad van master in de industriële wetenschappen: chemie



*Deze masterproef werd geschreven tijdens de COVID-19 crisis in 2020.
Deze wereldwijde gezondheids crisis heeft mogelijk een impact gehad op
de opdracht, de onderzoekshandelingen en de onderzoeksresultaten.*

FOREWORD

This dissertation is part of my master's thesis, the final challenge to take on my path as a chemical industrial engineer, and it researched photocatalysts with graphene under visual light irradiation.

This master's thesis turned out very differently than expected because of the virus, better known as COVID-19. A planned stay of almost five months in Hanoi, Vietnam was eventually reluctantly reduced to six weeks. As a result, it was not possible to actually carry out the planned experimental work, so only the written and theoretical part remained.

Despite the short stay, I would like to thank my promoters from Vietnam, Prof. Dr. Nguyen Hong Lien and Prof. Nguyen Duc Hoa for taking such good care of me and offering help when needed. I would also like to thank my promoter from Belgium, Prof. Dr. ir. Leen Braeken, for all the support and assistance she provided throughout the strange situation as well as the written part of the literature study.

Furthermore, I am grateful for the support and understanding of my family and friends. Specifically, my parents to always be there for me, my mom as proof-reader and finally my good friend and fellow student Leandro Schepers for joining me in this great and unforgettable adventure in Vietnam.

Kenneth Put
Diepenbeek, 2020

TABLE OF CONTENTS

Foreword.....	III
Table of contents.....	V
List of tables	VII
List of figures	IX
Abbreviations	XI
Abstract.....	XIII
Dutch abstract.....	XV
1. Project Design.....	1
1.1 Introduction	1
1.2 Problem Definition	1
1.3 Objectives	2
1.4 Materials & Methods.....	2
2. Literature study	5
2.1 Rhodamine B.....	5
2.2 Graphene	7
2.3 Photocatalysts.....	10
2.3.1 General	10
2.3.2 Requirements for a good photocatalyst.....	11
2.3.3 Photocorrosion.....	12
2.3.4 Bismuth oxyhalides as photocatalysts	13
2.3.5 Composites with bismuth oxyhalide photocatalysts	14
2.3.6 Photocatalytic mechanism of Fe ₃ O ₄ /BiOI@GO	16
2.4 Characterization	18
2.4.1 Scanning Electron Microscopy	18
2.4.2 Transmission Electron Microscopy	19
2.4.3 X-ray diffraction	20
2.4.4 Energy-Dispersive X-ray spectroscopy	22
2.4.5 Photoluminescence	22
2.4.6 Fourier-Transform Infrared spectroscopy	23
3. Experimental	25
3.1 Synthesis	25
3.2 Characterization	26
3.2.1 Theoretical results.....	26

3.3	Verification of the photocatalytic activity	29
	References	31

LIST OF TABLES

Table 1. Properties and dangers of Rhodamine B.....	6
Table 2. Results of different bismuth oxyhalide photocatalysts	15

LIST OF FIGURES

Figure 1. Molecular structure of triphenylmethane, the basis of triarylmethane colorants	5
Figure 2. Core molecular structure of Rhodamine	5
Figure 3. Synthesis of Rhodamine B	6
Figure 4. Different structures of graphene	7
Figure 5. Dirac cone present in graphene	8
Figure 6. Mechanism of photocatalysis	10
Figure 7. Oxidation reactions of h^+	10
Figure 8. Matlockite structure of bismuth oxyhalides	13
Figure 9. Energy levels of VB and CB versus momentum	14
Figure 10. Types of heterojunctions in semiconductor composites	15
Figure 11. Schematics of (a) the energy band position of Fe_3O_4 and BiOBr before contact, and (b) formation of a p–n junction after contact	16
Figure 12. Photocatalytic mechanism of $Fe_3O_4/BiOI@rGO$	17
Figure 13. Interactions by irradiation of a sample with an electron beam	18
Figure 14. Comparison of TEM and SEM	19
Figure 15. Influence of condenser apertures	20
Figure 16. Illustration of Bragg's Law	21
Figure 17. Standard XRD graph	21
Figure 18. Energy levels of fluorescence and phosphorescence	23
Figure 19. Reference XRD pattern of GO and graphene	27
Figure 20. EDX analysis of $BiOI/Fe_3O_4@GO$	27
Figure 21. PL spectra of Pristine GO	28
Figure 22. PL spectra of various concentrations of GO at pH = 4	28
Figure 23. Reference FTIR pattern of graphene and GO	29

ABBREVIATIONS

(r)GO	(reduced) graphene oxide
°	Degree
°C	Degree Celsius
μm	Micrometre
2D	Two-dimensional
3D	Three-dimensional
A	Electron acceptors
AOP	Advanced Oxidation Process
BiOI/Fe ₃ O ₄ @(r)GO	Bismuth iodide oxide + Iron(II,III) oxide + (reduced) graphene oxide
BiOX	Bismuth oxyhalides
BSE	Backscattered electrons
CB	Conduction band
D	Electron donor
d	Lattice spacing
e ⁻	Electron
EDX	Energy-Dispersive X-ray spectroscopy
eV	Electron volt
FTIR	Fourier-Transform Infrared spectroscopy
g/L	Gram/litre
GO	Graphene oxide
h ⁺	Hole
HUST	Hanoi University of Science and Technology
ITIMS	International Training Institute for Materials Science
MEMS	Micro-electromechanical systems
mg/L	Milligram/litre
min	Minute
MO	Methyl Orange
n	Integer
nm	Nanometre
NOR	Norflaxin
PL	Photoluminescence
rGO	Reduced graphene oxide
RhB	Rhodamine B
SCE	School of Chemical Engineering
SE	Secondary electrons
SEM	Scanning Electron Microscopy
TEM	Transmission Electron Microscopy
UV	Ultraviolet
V	Acceleration voltage
VB	Valence band
wt%	Weight percentage

XRD

θ

λ

X-ray Diffraction

Diffraction angle

Wavelength

ABSTRACT

Photocatalysts have applications in the degradation of organic pollutants. However, there are still several disadvantages associated with photocatalysts, such as low activity in the visible light spectrum and a fast recombination of electron hole pairs. This paper investigates bismuth iodide oxide + iron(II,III) oxide + (reduced) graphene oxide (BiOI/Fe₃O₄@(r)GO) as a photocatalyst to determine whether it overcomes these drawbacks. Based on literature bismuth oxyhalides show excellent photocatalytic behaviour by themselves. The role of Fe₃O₄ as a magnetic component is to ensure easy separation during synthesis on the one hand and on the other hand improving the absorption of visible light. (r)GO should also ensure a better absorption of visible light, and because it is known as a material with a very high electron mobility it should reduce recombination as well. Experiments will show if Fe₃O₄ and (r)GO can fulfil their respective roles.

The experimental set-up designed for the validation of the research hypothesis included characterisation using Scanning Electron Microscopy, Transmission Electron Microscopy, X-ray Diffraction, Fourier-Transform Infrared spectroscopy, Energy-Dispersive X-ray spectroscopy and photoluminescence and verification of the photocatalytic activity in a degradation experiment with Rhodamine B by means of optical absorbance measurements under visible light irradiation. Unfortunately, due to the COVID-19 crisis, these experiments could not be executed.

DUTCH ABSTRACT

Fotokatalysatoren hebben toepassingen in de afbraak van organische verontreinigingen. Er zijn echter nog steeds verschillende nadelen verbonden aan fotokatalysatoren, zoals lage activiteit in visueel licht en snelle recombinitie van elektrongatparen. Deze paper onderzoekt bismutjodide-oxide + ijzer(II,III)oxide + (gereduceerd) grafeenoxide ($\text{BiOI}/\text{Fe}_3\text{O}_4@(\text{r})\text{GO}$) als katalysator om na te gaan of het deze nadelen overwint. Volgens de literatuur vertonen bismut oxyhaliden op zichzelf uitstekend fotokatalytisch gedrag. De rol van Fe_3O_4 als magnetische component is enerzijds te zorgen voor een makkelijke scheiding tijdens synthese en anderzijds absorptie van visueel licht te verbeteren. (r)GO moet ook zorgen voor betere absorptie van visueel licht en omdat het gekend is als materiaal met een zeer hoge elektronmobiliteit moet het ook recombinitie verminderen. Experimenten zullen aantonen of Fe_3O_4 en (r)GO hun respectievelijke rollen kunnen vervullen.

De experimentele opzet voor de validatie van de onderzoekshypothese omvatte karakterisering met behulp van Scanning Electron Microscopy, Transmission Electron Microscopy, X-ray Diffraction, Fourier-Transform Infrared spectroscopy, Energy-Dispersive X-ray spectroscopy en fotoluminescentie en verificatie van de fotokatalytische activiteit in een degradatie-experiment met Rhodamine B door middel van optische absorptiemetingen onder zichtbare lichtbestraling. Helaas konden deze experimenten als gevolg van de COVID-19-crisis niet worden uitgevoerd.

1. PROJECT DESIGN

1.1 Introduction

The Hanoi University of Science and Technology (HUST), founded in 1956, is the first multidisciplinary technical university of Vietnam. HUST is a university which holds high regards for academic excellence and effectiveness. Dedication and commitment from the staff as well as the students is highly valued, and mutual respect and integrity are also a part of their core values [1]. The institute where this academic research takes place is the International Training Institute for Materials Science (ITIMS) and the School of Chemical Engineering (SCE). Scientific education, research and transfer of technological knowledge in the field of materials science are accomplished in this establishment [2]. Important lines of research of this institute are: biological and electrochemical sensors, types and applications of magnetic materials, opto-electronic and photonic materials, superconducting materials at high temperature, micro-electromechanical systems (MEMS), and biological composite materials. My specific case falls under conducting research on a material called graphene.

1.2 Problem Definition

Graphene is a 2D carbon-based material with a honeycomb sp^2 carbon lattice [3], [4], [5], [6]. It was first isolated in 2004 by Andre Geim and Konstantin Novoselov, they succeeded by using a method now known as the “Scotch tape method”. This is a simple but effective method to obtain graphene from bulk graphite. By attaching a piece of scotch tape to a solid block of graphite and then removing it followed by dissolving the tape itself, graphene is obtained. Graphene has applications in composites, coatings, sensors, electronics and more [4], [7].

The past sixteen years have seen an increasing amount of research regarding graphene. This is due to the high number of remarkable properties that graphene possesses. The material is only one atom thick, it is the strongest material on earth and yet it is very flexible. Besides, it has the highest known thermal conductivity, it is electrically highly conductive and it is also transparent which leads to even more possible applications. Despite all these characteristics, graphene has not made a breakthrough in all corners of the industry as it is still difficult to produce on a large scale [6], [8], [9], [10], [11].

In the form of composites, graphene has an application as a photocatalyst. Photocatalysts are catalysts that utilize energy from light to drive chemical conversions. Semiconductors such as metal-oxides absorb a photon of light to promote an electron (e^-) from the valence band (VB) to the conduction band (CB) leaving a hole (h^+) in the VB. This system of electrons and holes is necessary to enable photocatalysts to work as a degradation method because they are responsible for the redox reactions that need to take place [12].

There are a number of drawbacks to popular photocatalysts. One possibility is that photocatalysts show low activity in visible light. It is also probable that the formed electron-hole pairs may not be stable and quickly recombine leading to reduced photocatalytic activity.

Composites of graphene and metal-oxides show promising results for both disadvantages [12], [13].

1.3 Objectives

The main aim of this study is to synthesize and characterize a graphene/metal-oxide composite which can act as a reusable photocatalyst under visible light irradiation for the degradation of different concentrations of an organic pollutant (Rhodamine B). The degradation should stay effective even after 10 cycles with the same catalyst.

Bismuth iodide oxide + iron(II,III) oxide + (reduced) graphene oxide will be used as catalyst. There are several reasons for this. Namely, BiOBr-Fe₃O₄ can degrade an antibiotics solution of 10 mg/L Norflaxin (NOR) for more than 99% in 30 min [14]. This is already a promising result, but the reported concentration of 10 mg/L is rather low, making a composite with graphene could lead to higher degradable concentrations. Graphene would also lead to less recombination of electron hole pairs.

A second reason is that studies showed that BiOI is the most effective bismuth halogen oxide for degradation under visual light irradiation. As a result, this research will be conducted with BiOI instead of BiOBr [15].

Fe₃O₄ as a magnetic component ensures that the catalyst can be easily separated during synthesis as well as from solutions with the degradable component. This reduces the cost of separation processes [12].

Variables in the experiments are making the catalyst with graphene oxide on the one hand and with reduced graphene oxide on the other hand. Their weight percentages will also be varied between 2 and 6 weight percentage. The catalyst loading will be tested between 50 and 400 mg/L and the pollutant concentration will change between 10-50 mg/L. For recycling efficiency, several cycles will be performed with the same catalyst sample.

Catalysts are evaluated based on their photodegradation efficiency and their recycling efficiency. A comparison is also made between rGO and GO.

1.4 Materials & Methods

The research will be divided into three distinct parts: Synthesis, Characterization and Verification of photocatalytic activity.

The synthesis of graphene oxide and reduced graphene oxide will be performed according to an ultrasonication-assisted modified Hummers' method. In this method, graphite and a mixture of concentrated sulphuric acid and concentrated nitric acid are combined. Reaction occurs between these chemicals in presence of potassium permanganate as a catalyst. After this reaction step the mixture is kept under ultrasonication to improve the exfoliation of graphene oxide.

Before the desired composite can be created, iron(II,III) oxide has to be synthesized. This is done by reacting $\text{FeCl}_3 \cdot 6\text{H}_2\text{O}$, PEG 6000 and CH_3COONa , dissolved in ethylene glycol solution, at elevated temperature. Afterwards, the black precipitates can be collected, cleaned and dried in vacuum to obtain Fe_3O_4 .

The coveted composite can now be synthesized by adding the previously prepared products together in combination with $\text{Bi}(\text{NO}_3)_3 \cdot 5\text{H}_2\text{O}$, KI and CH_3COONa . This also requires ultrasonication, washing and drying steps [12], [13], [16].

In the second part of the research, the formed composite will be characterized by multiple analytical methods. Scanning Electron Microscopy and Transmission Electron Microscopy analysis will result in clear images that will provide morphological and compositional information. X-ray Diffraction will be used to analyse the crystal structure. Fourier-Transform Infrared spectroscopy will give more information on functional groups, this is important to verify the reduction step. Energy-Dispersive X-ray spectroscopy will be carried out for elemental analysis of the samples. Finally, photoluminescence characterizes the electronic and optical properties.

Ultimately, the photocatalytic activity of the composite will be verified under visible light irradiation in a degradation experiment with Rhodamine B using optical absorbance measurements. By measuring the absorbance, the concentration of Rhodamine B can be obtained at various times and the degradation percentage over time can be calculated. This procedure will be executed for different starting concentrations of the organic pollutant to find the maximum degradable concentration. Catalysts will be tested on their recycle efficiency as well by conducting multiple catalytic cycles with the same catalyst [17].

2. LITERATURE STUDY

2.1 Rhodamine B

Rhodamines are a group of colouring agents, more specifically a subdivision of triarylmethane colorants [3], [18], [19], [20], [21]. A dye must have the following triphenylmethane structure to belong to the triarylmethane colorants:

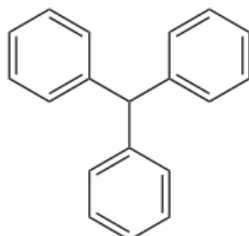


Figure 1. Molecular structure of triphenylmethane, the basis of triarylmethane colorants [22]

To be a part of the Rhodamine family, the molecule must possess the structure in Figure 2. This core molecular structure of Rhodamine contains the triphenylmethane group as well as an oxygen atom bound between 2 phenyl groups. The phenyl groups to which this oxygen atom is bound must both possess a nitrogen atom in meta of the oxygen atom.

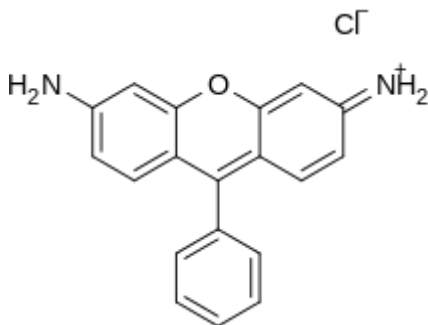


Figure 2. Core molecular structure of Rhodamine [23]

Rhodamines are synthesized by reaction of phthalic anhydride with an amino derivative of phenol. They have applications as colouring agents for paper and inks, but also as photochemicals and tracer dyes in fluorescence microscopy [24].

The following section examines Rhodamine B in more detail. Rhodamine B is the Rhodamine which is obtained by combining two molecules of 3-(Di-ethylamino)phenol and phthalic anhydride under the influence of heat and sulphuric acid as catalysts [23]. The synthesis is terminated by the addition of hydrochloric acid as can be seen in Figure 3.

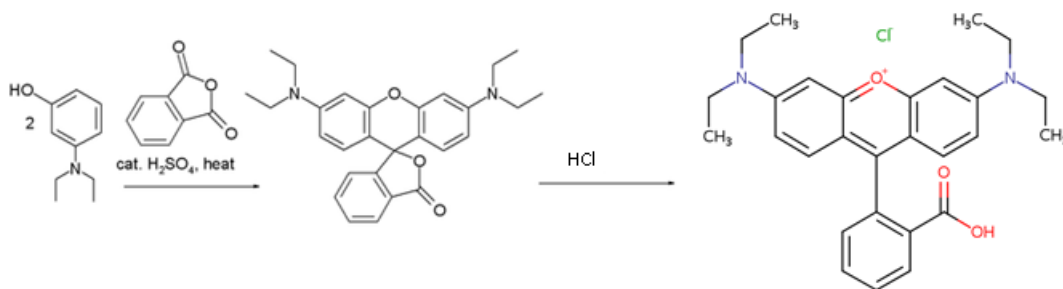




Figure 3. Synthesis of Rhodamine B

Animal tests have shown RhB to be a carcinogenic substance and in California it is suspected to be carcinogenic for mankind as well. Because of the dangers shown in Table 1 and its carcinogenic properties, RhB should not be discharged by industries in waterways. So degradation is a solution to this problem. If complete mineralization occurs, the end products of RhB will be water and carbon dioxide but getting the RhB concentration below a certain threshold will suffice [4], [18].

Table 1. Properties and dangers of Rhodamine B [25]

Molecular formula	$C_{28}H_{31}ClN_2O_3$
Solvability in water	12 g/L at 25°C
Colour	Red-pinkish
Hazard pictograms	GHS05:  GHS07: 
Personal Protective Equipment	Dust mask type N95 Eyeshields Gloves

RhB is also used for analytical applications, it can be wielded as a determination agent for gallium in minerals and ores, thallium in foods and minerals and many more [26].

2.2 Graphene

Graphene is a 2D carbon-based material with a honeycomb sp^2 carbon lattice. It was first isolated in 2004 by Andre Geim and Konstantin Novoselov, they succeeded by using a method now known as the “Scotch tape method”. This is a simple but effective method to obtain graphene from bulk graphite. By attaching a piece of scotch tape to a solid block of graphite and then removing it followed by dissolving the tape itself, graphene is obtained. Graphene has applications in composites, coatings, sensors, electronics and more [3], [4], [5], [6], [7], [27], [28], [29].

The past sixteen years have seen an increasing amount of research regarding graphene. This is due to the high number of remarkable properties that graphene possesses. The material is only one atom thick, and one can obtain it in various forms through functional groups. For example, pristine graphene has no functional groups, it consists entirely of carbon atoms. A drawback is that this is difficult to synthesize, only small yield percentages can be obtained when synthesizing this material. Easier to synthesize is graphene oxide which contains many epoxides and hydroxyl groups as illustrated in Figure 4. Reduction of this graphene oxide results in reduced graphene oxide in which all epoxides and a large part of the hydroxyl groups are reduced. All these different structures of graphene can be used as photocatalysts, but the purer the material the better the performance of the photocatalyst. An assessment based on economic and qualitative aspects will prove to be necessary [6], [8], [9], [30].

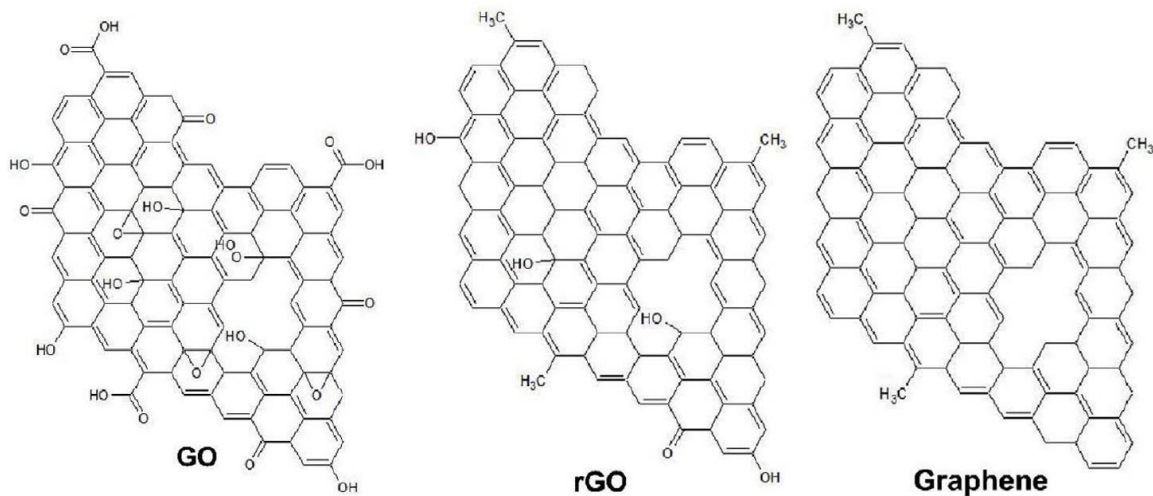


Figure 4. Different structures of graphene [9]

Due to their structure, graphene materials have a large surface area, the largest compared to other materials. It is also the strongest material on earth and yet very flexible. The strength comes from the strong covalent bonds between the carbon atoms. The flexibility is due to the possibility of stretching these covalent bonds, here the hexagons are no longer regular. Besides, it has the highest known thermal conductivity, it is electrically highly conductive because of the extraordinarily high electron mobility caused by the Dirac cones and it is also transparent which leads to even more possible applications. Despite all these characteristics, graphene has not made a breakthrough in all corners of the industry as it is still difficult to produce on a large scale [6], [8], [9].

As previously pointed out, Dirac cones characterize the electronic structure of graphene. The cone in Figure 5 represents linear energy dispersion at Fermi level.



Figure 5. Dirac cone present in graphene [31]

The CB and the VB connect at points known as Dirac points. These points lead to graphene having massless fermions. It is because of these massless fermions that graphene possesses ultra-high charge carrier mobility. Because the CB and the VB connect at this Dirac point, graphene is a zero band gap semiconductor [32].

The most common method to synthesize graphene oxide is to use Hummers' method. This method falls under liquid phase exfoliation, other techniques are micro-mechanical exfoliation, chemical vapour deposition and epitaxial growth.

Hummers' method was developed by Hummers in 1958 based on the work of Brodie and Staudenmaier. The method involves the addition of graphite and sodium nitrate to sulphuric acid at 66°C. This solution is then cooled to 0°C after which KMnO_4 is slowly added and the temperature must not exceed 20°C. On the one hand this is a safety measure because if the temperature is not regulated the reaction vessel could catch on fire. On the other hand, a higher temperature is unfavourable because a slow oxidation process is wanted so that more oxygen ends up in between the graphite layers. Finally, water is added to this mixture and the solids can be isolated and purified [33], [34].

The development of this method led to the shortening of the synthesis time of graphene oxide. Hummers' method is of course not without its shortcomings, because it is not the most efficient and environmentally friendly method. The C/O ratio in the Hummers' method (2.25) is lower than the C/O ratio in Staudenmaier's method (2.89) and the addition of NaNO_3 has a negative environmental role, which is why nowadays, there are known modified Hummers' methods that remove the use of sodium nitrate or use exfoliation and ultrasonic waves for a higher efficiency [7], [9].

The synthesis of graphene oxide and reduced graphene oxide in this study will be performed according to an ultrasonication-assisted modified Hummers' method. In this method, graphite and a mixture of concentrated sulphuric acid and concentrated nitric acid are combined. Reaction occurs between these chemicals in presence of potassium permanganate as a

catalyst. After this reaction step the mixture is kept under ultrasonication to improve the exfoliation of graphene oxide.

Before the desired composite can be created, iron(II,III) oxide has to be synthesized. This is done by reacting $\text{FeCl}_3 \cdot 6\text{H}_2\text{O}$, PEG 6000 and CH_3COONa , dissolved in ethylene glycol solution, at elevated temperature. Afterwards, the black precipitates can be collected, cleaned and dried in vacuum to obtain Fe_3O_4 .

The coveted composite can now be synthesized by adding the previously prepared products together in combination with $\text{Bi}(\text{NO}_3)_3 \cdot 5\text{H}_2\text{O}$, KI and CH_3COONa . This also requires ultrasonication, washing and drying steps [12], [13], [16].

Due to its remarkable properties, graphene has many possible applications, but there are also a number of known disadvantages of graphene. Strong π - π interactions make it possible for irreversible agglomeration to occur, this results in the good properties being limited because graphene possesses these properties only in structures of a few layers. The solution to this problem is to make composites with polymers and metals. During synthesis, ultrasonic waves can be used to further prevent agglomeration. In these composites, the properties of graphene are retained and therefore the final composite contains better properties than the original polymer/metal. For example, graphene composites have applications such as photocatalysts and adsorbents. This will be further discussed in the section 'Photocatalysts' [4], [35], [36].

2.3 Photocatalysts

2.3.1 General

Photocatalysts utilize energy from light to drive chemical conversions. They are catalysts so they themselves come out of the reaction process unchanged. Semiconductors absorb a photon of light to promote an e^- from the VB to the CB leaving a h^+ in the VB. This can only occur when the energy from the photon is equal to or larger than the bandgap of the photocatalyst. When these charge carriers reach the surface by means of charge transportation, redox reactions can take place with absorbed pollutants as can be seen in Figure 6.

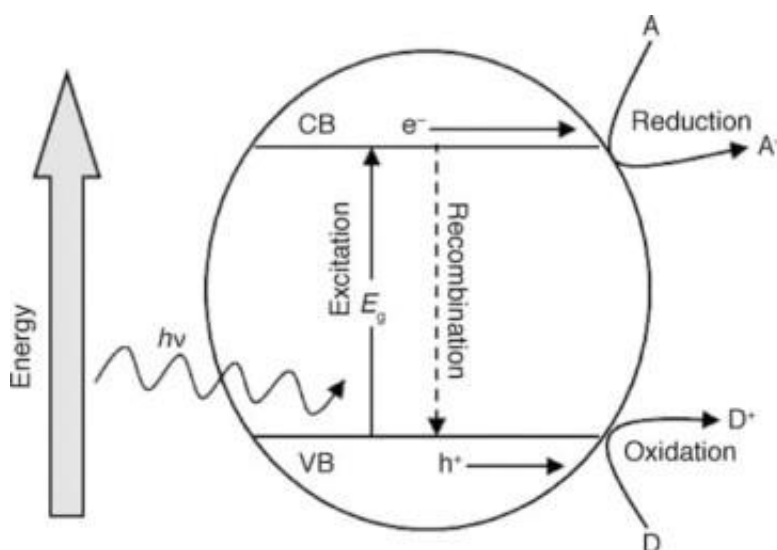


Figure 6. Mechanism of photocatalysis [37]

These redox reactions will occur because a hole, h^+ , has a high oxidation potential. This hole can therefore either cause indirect oxidation by the formation of hydroxyl radicals or direct oxidation by reaction with the pollutant itself. An OH radical is the most oxidizing compound that exists. Basically, a positive hole will react with an electron donor (D) at the surface of the photocatalyst. In principle, photocatalysts work as advanced oxidation processes (AOP) with positive holes as initiator. Possible reactions that can occur can be seen in Figure 7 [38], [39], [40].

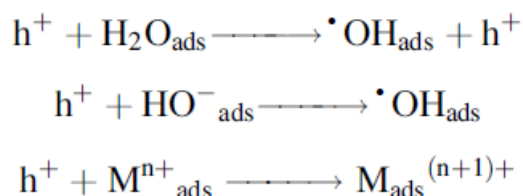


Figure 7. Oxidation reactions of h^+

According to the definition of a redox reaction, there must of course also be a reduction. The electrons will react with electron acceptors represented as A in Figure 6 at the surface of the

photocatalyst. If this does not happen there will be a build-up of negative charge which is unwanted in the mineralization process. The removal of electrons will increase the efficiency of photocatalysts. Oxygen can be used as a profitable way to do this. After reaction of this oxygen with the electron, it can react further until eventually a hydroxyl radical is formed. This in turn can act as an oxidizing compound.

Normally in oxidative processes hydrogen peroxide has to be added for the production of hydroxyl radicals, but the fact that these OH radicals are formed from water in reaction with h^+ and oxygen in reaction with e^- means that hydrogen peroxide does not have to be dosed. This also means that no hydrogen peroxide has to be stored which is beneficial for the safety of the process since this is a dangerous substance.

Recombination of these electron-hole pairs is possible before reaction can take place. Heat will be released due to this recombination. Fast recombination is one of the disadvantages of photocatalysts. It must therefore be ensured that these electron-hole pairs exist long enough so that they can be moved to the surface of the catalyst to start the redox reaction. Graphene can be used as a support because it has a very high electron mobility which can move the charge carriers to the surface [38], [41], [42].

These semiconductor photocatalysts, typically metal oxides, can completely mineralize and degrade pollutants, this way H_2O and CO_2 are left as end products. They also have a good track record for very stable pollutants which are hard to degrade by other means.

Adsorption, coagulation, electrochemical methods, sonochemical treatment and ultrafiltration are all techniques to process wastewater other than photocatalysis. But in comparison with these processes, photocatalysis is a quick, inexpensive and ecological strategy to combat wastewater pollution as there are no waste disposal problems. In the case of adsorption for example, the pollution is transported from one medium to another. While in photocatalysis the pollutant is actually broken down [15]. Pressure and temperature conditions do not need to be increased during the photocatalytic process which makes this a fast process.

If these photocatalysts are active under visual light, then this gives a clear ecological and industrial advantage. After all, solar energy is a green, non-polluting source of energy and if it can be used efficiently, there is no need for an external light source. With efficient photocatalysts one can perform water splitting and carbon dioxide reduction.

2.3.2 Requirements for a good photocatalyst

A photocatalyst has to meet several requirements to be considered a good catalyst. Different requirements are: it must be easy to synthesize, cheap, non-toxic, chemically and biologically stable, even against photocorrosion. Its activity in the wavelength spectrum is another important factor as discussed earlier and there is a certain wanted band gap for different industrial situations. In applications where a high-energy lamp is available as a light source, the band gap may be larger. Fewer restrictions could provide an economic advantage, but the fact that the lamp uses a lot of energy is economically disadvantageous. Visible light, such as the sun, as a source gives an ecological advantage but this requires a smaller band gap which is economically more disadvantageous. For different applications, a trade-off will have to be made based on degradation efficiency and economic efficiency.

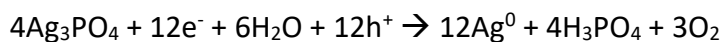
Reusability and surface area are significant features of the catalyst [43]. The choice is obvious if one catalyst can be used only once but another catalyst can be used over a hundred times. The greater the surface area, the more active sites for degradation the catalyst possesses [15].

The best known and most studied photocatalyst is titanium dioxide, because it contains good properties such as low cost, non-toxicity, good stability and high activity under UV light. Despite these good properties, TiO₂ has some disadvantages. It has a low activity under visible light because it has a high band gap of 3.2 eV and recombination of the electron-hole pairs occurs quickly [14], [44], [45]. For these reasons modification of TiO₂ photocatalysts has already been thoroughly studied, the combination of graphene and TiO₂ was also scrutinized. This has shown that the combination between photocatalysts and reduced graphene oxide results in enhanced photocatalytic performances. In general, doping reduces the band gap and required wavelengths shift toward the visible light spectrum. This obviously improves photocatalysis under visible light irradiation. Doping also leads to impurities and more oxygen vacancies [37].

2.3.3 Photocorrosion

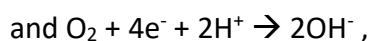
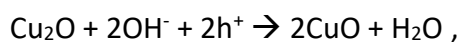
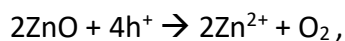
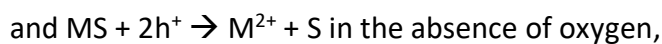
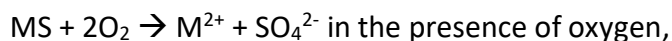
Returning to the subject of photocorrosion, this can be brought about through multiple mechanisms of which the decomposition of the semiconductor by the generated electrons and holes is the cause.

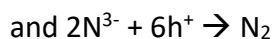
Silver containing composites such as Ag₃PO₄ suffer from photogenerated-electron-induced instability, these electrons will reduce Ag⁺ which dissolves the compounds structure according to the following overall reaction:



This process will lead to reduced efficiency and eventually deactivation of the catalyst.

Photogenerated-hole-induced instability is a second possibility, in this process the holes will oxidize and decompose the photocatalyst. Catalysts that are susceptible to this type of photocorrosion are metal sulfides, zinc oxide, copper oxide and metal oxynitride semiconductors [46], [47] with:





as respective occurring reactions.

2.3.4 Bismuth oxyhalides as photocatalysts

The photocatalysts this study will be focusing more on are bismuth oxyhalides, which, thanks to their suitable electric and optical properties possess eminent photocatalytic behaviour. Bismuth oxyhalides are represented by BiOX where X can be chlorine, iodine, bromine or fluorine. The structure of bismuth oxyhalides, which falls under a group of V-VI-VII ternary oxide semiconductors, provides very good separation of formed electron hole pairs. Their crystal structure is a tetragonal matlockite structure which consists of stratified $[\text{X-Bi-O-Bi-X}]$ layers kept together by Van Der Waals interactions and strong intralayer covalent bonds as can be seen in Figure 8. Each bismuth atom in this structure is surrounded by four oxygen atoms and four halogen atoms. Internal electrical fields are also present because of the matlockite structure. These electric fields are located perpendicular to the layers, which may have a positive influence on the separation of charge carriers [48].

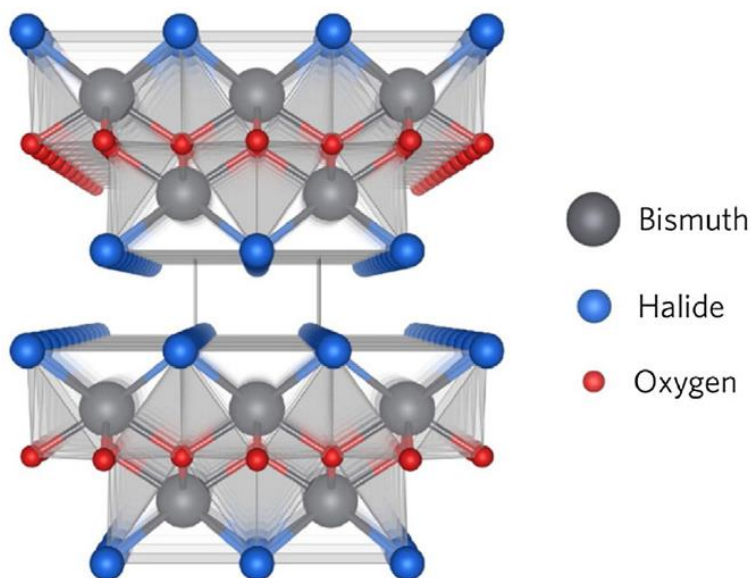


Figure 8. Matlockite structure of bismuth oxyhalides [49]

Of course the bismuth oxyhalides also differ from each other. For example, the band gaps of chlorine and iodine have a value of 3.5 eV and 1.63-2.1 eV respectively. Bismuth iodide oxide has the lowest band gap out of all the BiOX 's but it is reported that recombination occurs quicker in BiOI . Despite the fact that recombination happens faster than with other bismuth oxyhalides, this does not cause any problems [15]. BiOI has an indirect band gap which reduces recombination compared to photocatalysts with a direct band gap [12]. For a direct bandgap, the momentum of the maximum in the VB and the minimum of the momentum in the CB have the same value. Figure 9 shows this graphically.

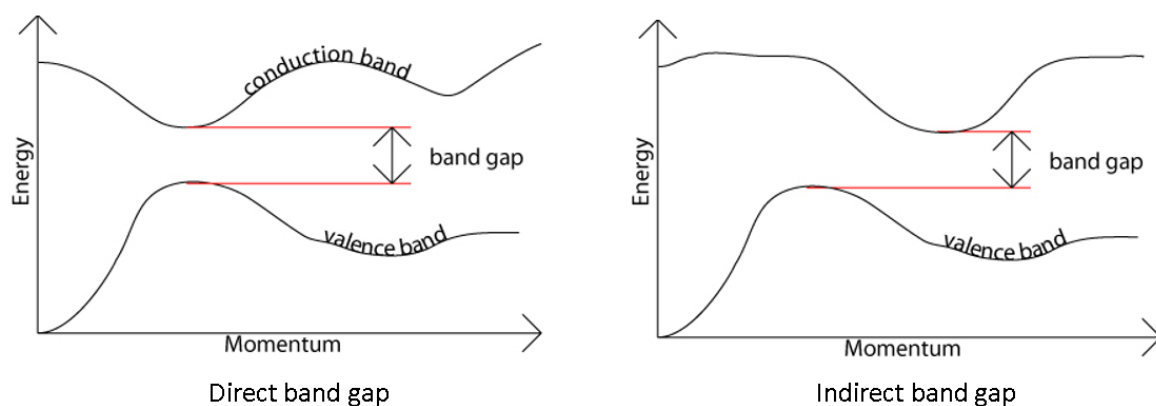


Figure 9. Energy levels of VB and CB versus momentum [50]

The momentum in the x-axis of Figure 9 refers to the crystal momentum of the electrons, meaning that direct band gap semiconductors can directly emit a photon but recombination will occur directly and fast as well. Only light will be released during this recombination as there has not been any change in kinetic energy or momentum of the electron. For indirect band gap semiconductors, the electrons must enter an intermediate state by transferring momentum to the crystal lattice before excitation can occur. Excitation happens in the form of heat in the case of indirect band gap semiconductors and charge carrier life exceeds that of direct band gap semiconductors [50], [51].

It is reported that BiOBr has the highest photocatalytic activity under UV irradiation, but BiOI shows the best degradation efficiency under visible light irradiation. For these reasons, the experimental phase would have been performed with BiOI. In order to solve recombination problems and improve the photocatalysts, metal/non-metal doping and coupling with other semiconductors were sought as a solution [15].

2.3.5 Composites with bismuth oxyhalide photocatalysts

BiOI was coupled to three different forms of graphene, the composites in these experiments were all synthesized via a hydrothermal method. Combinations were made with graphene, 3D graphene and rGO. Optimal results of these combinations were respectively six times, seven times and six times better than naked BiOI. And here the optimal weight percentages of the graphene component varied from 2% to 6%. The improved results are due to the excellent electron mobility of graphene, as shown in

Table 2 [12], [15].

Table 2. Results of different bismuth oxyhalide photocatalysts [14], [15]

Sample	Pollutant		
Sample	BiOI/GR	Pollutant	Methyl Orange (MO)
Method	Hydrothermal (120°C for 6 h)	Light source	500 W Xe lamp
Optimal sample	2 wt% BiOI/GR	Concentration	0.05 g/50 mL of 10 mg/L MO sol.
Band gap _{Naked BiOI}	1.72 eV	% deg. (Naked BiOI)	28% in 4 h
Band gap _{optimal}	1.52 eV	% deg. (optimal)	88% in 4 h
Sample	3D GR/BiOI	Pollutant	RhB
Method	In situ crystallization	Light source	1000 W Xe lamp
Optimal sample	5 wt% 3D GR/BiOI	Concentration	0.05 g/50 mL of 3 x 10 ⁻⁵ M/L RhB sol.
Band gap _{Naked BiOI}	1.72 eV	% deg. (Naked BiOI)	34% in 4 h
Band gap _{optimal}	1.11 eV	% deg. (optimal)	76% in 4 h
Sample	BiOI/rGO	Pollutant	MO
Method	Hydrothermal (150°C for 8 h)	Light source	250 W Xe lamp
Optimal sample	6 wt% BiOI/rGO	Concentration	80 mg/80 mL of 10 mg/L MO sol.
Band gap _{Naked BiOI}	1.86 eV	% deg. (Naked BiOI)	29% in 4 h
Band gap _{optimal}	1.64 eV	% deg. (optimal)	85% in 4 h
Sample	BiOBr/Fe ₃ O ₄	Pollutant	NOR
Method	Direct mixing	Light source	800 W Xe lamp
Optimal sample	/	Concentration	1 g/L of 10mg/L NOR sol.
Band gap _{Naked BiOBr}	/	% deg. (Naked BiOBr)	/
Band gap _{optimal}	/	% deg. (optimal)	>99% in 30 min

Coupling with other semiconductors is also a promising way to improve BiOI photocatalysts. Semiconductor/semiconductor heterojunctions can appear. These are found in 3 configurations as shown in Figure 10. Error! Reference source not found..

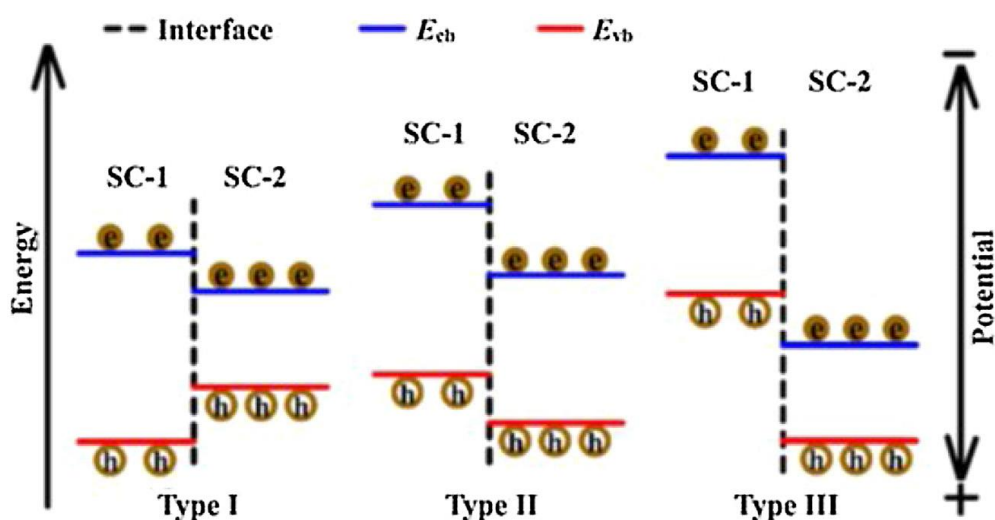


Figure 10. Types of heterojunctions in semiconductor composites [52]

Only a heterojunction of Type II is beneficial because it distributes the positive holes and the negative electrons over the two semiconductors. With a heterojunction of Type I, recombination of electrons and holes will occur in SC-2 because it is most beneficial for both the holes and the electrons to be in SC-2. And with a heterojunction of Type III there is no overlap between the band gaps of the semiconductors so no migration of electrons can occur before contact of the semiconductors. However, when two semiconductors do come in contact the bands will reform. This is shown in Figure 11 for BiOBr and Fe₃O₄. In this process the Fermi energies (E_F) have to be aligned after which the bands will be bent. Now electrons and holes can and will migrate from one semiconductor to the other [53], [54], [55].

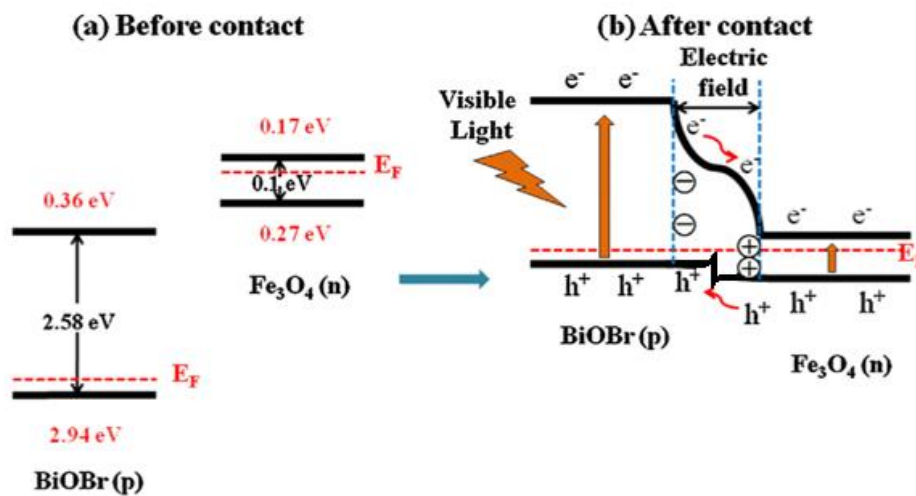


Figure 11. Schematics of (a) the energy band position of Fe₃O₄ and BiOBr before contact, and (b) formation of a p–n junction after contact [55]

The combination of BiOI and Fe₃O₄ belongs to Type III, so at first sight, before contact, a composite of these two semiconductors does not offer any advantage. Yet, this is what would be tested because the bands will reform and Fe₃O₄ as a magnetic component offers a different advantage to the system [15]. By adding Fe₃O₄ as a magnetic semiconductor, the photocatalyst can be magnetically separated to reduce synthesis time while this would normally be done via sedimentation and centrifugation, which are time-consuming processes [12].

2.3.6 Photocatalytic mechanism of Fe₃O₄/BiOI@GO

Singh et al. [12] explored the photocatalytic mechanism of Fe₃O₄/BiOI@GO in their work. There are some inconsistencies in their explanation since the CB and VB energy levels are given different values in their explanation and in their illustration, but the overall proposed mechanism stays the same. They mention that, for BiOI, the CB minimum has a value of 0.58 eV and the VB maximum has a value of 2.30 eV. In Figure 12 can be seen that the CB minimum has a value of 0.79 eV and the VB maximum of 2.64 eV. So this is something that certainly needs to be looked into in this investigation.

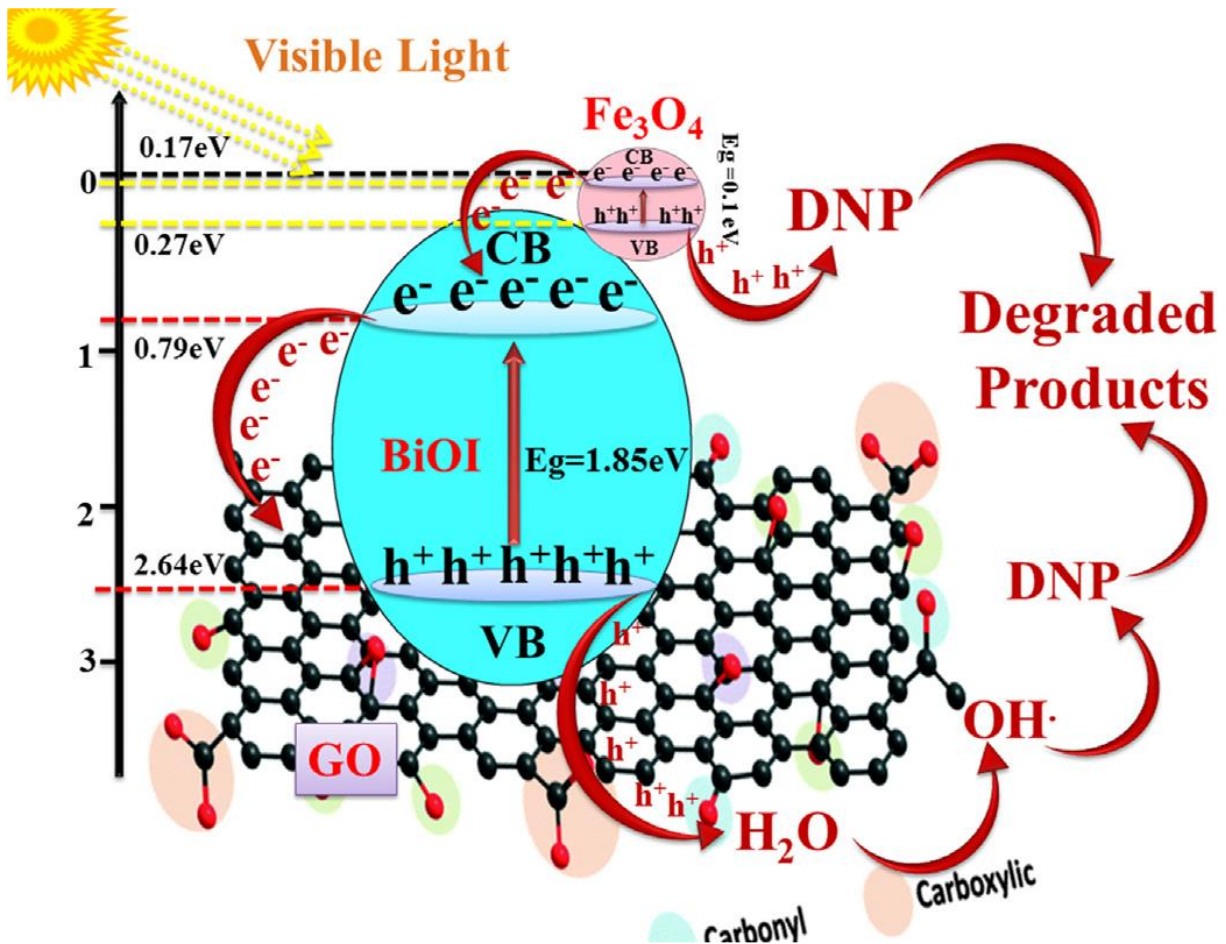


Figure 12. Photocatalytic mechanism of $\text{Fe}_3\text{O}_4/\text{BiOI}@(\text{r})\text{GO}$ [12]

On to the mechanism, both BiOI and Fe_3O_4 will generate holes and electrons through photoexcitation. The narrow band gap of Fe_3O_4 , located between 0.17 and 0.27 eV, enhances the absorption of visible light. When appropriate/adequate light energy is introduced into the composite, the electrons can be transferred from the CB of Fe_3O_4 to the CB of BiOI because of the reformed bands. This leads to the separation of charge carriers in Fe_3O_4 . The electrons in the CB of BiOI can then be transferred to the (r)GO leading to separation of charge carriers in BiOI as well. Radicals will then be produced and the pollutant will be degraded according to the previously discussed reactions [12].

2.4 Characterization

The section below describes what each analytical technique actually entails, including its principle, the sample requirements and possible sample preparation, and applications.

2.4.1 Scanning Electron Microscopy

SEM forms a 3D image by moving a focused electron beam across the surface of solid specimens. This electron beam will interact with a thin layer on the surface of the sample (a few μm maximum). The image is formed by measuring the result of the interaction. As can be seen in Figure 13, different interactions take place when the electron beam hits the sample [56], [57].

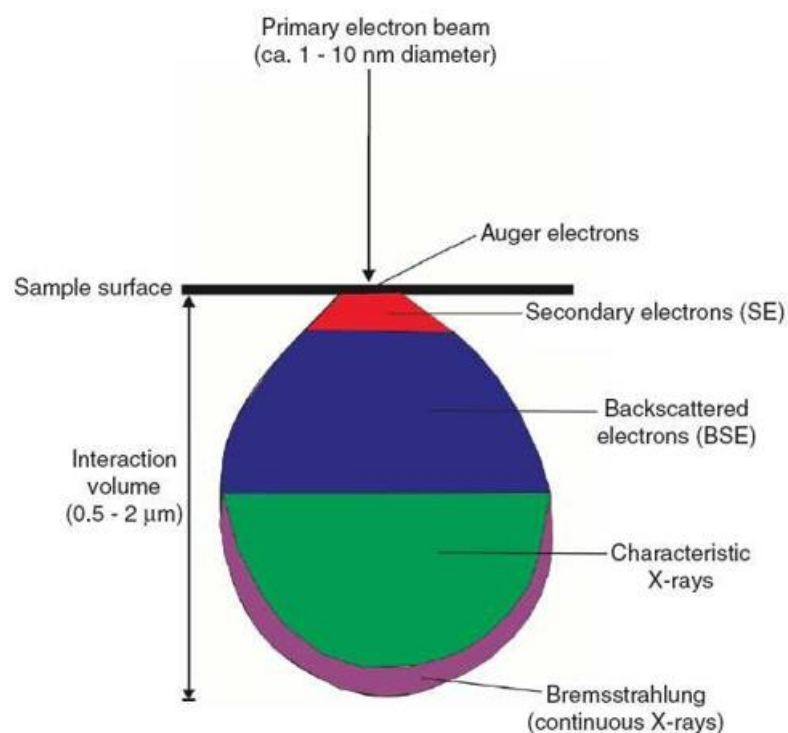


Figure 13. Interactions by irradiation of a sample with an electron beam [58]

Some of these interactions can be used for imaging. Backscattered electrons (BSE), secondary electrons (SE) and characteristic X-rays will be discussed.

When a primary e^- with great amounts of kinetic energy falls on the surface of the specimen it can knock an e^- from its place, these are then known as the SE and they only have a maximum kinetic energy of 50 eV. The yield of these SE depends on the acceleration voltage V . The depth and lateral width are roughly proportional to V^2 and $V^{3/2}$ respectively. The SE electrons will vary for different atoms, atoms with a higher atom number will have a smaller depth but the lateral width will be higher than for atoms with a smaller atom number. The resulting image will give a visualization of the texture of the surface and the roughness in which bismuth, iron and carbon will be clearly distinguishable.

A primary electron can undergo deflection instead of knocking another electron from its place. These primary electrons will then leave the surface with only a small change in their kinetic energy. These are the BSE and they possess high energy. The yield of these electrons is independent of V and small in comparison to the SE yield. It is very dependent on the atom

number though, the higher the atom number the higher the BSE yield. BSE will give information on the composition, the topography and the crystal structure of the specimen. When excited electrons fall back to lower energy levels, they produce characteristic X-rays for each element in the sample that got excited by the electron beam [56], [59].

This electron beam provides intense irradiation and can even damage the sample, but in general SEM is seen as 'non-destructive'. Electron microscopes are vacuum based instruments, so the samples need to be able to handle vacuum as well. The accumulation of electrostatic charge has to be prevented by making the surface of the specimen electrically conductive and electrically grounded. If all these requirements are met, SEM can be used to create images of surfaces down to 50 nm in size with a resolution between 1-20 nm [56].

2.4.2 Transmission Electron Microscopy

TEM is capable of forming a highly magnified 2D image with a much higher resolution than SEM by using an electron beam. This electron beam is focused using a condenser lens, afterwards it passes through the sample as the name suggests. For this reason, samples used in TEM have to be cut very thin whereas in SEM this is not necessary. High angle diffracted electrons can be blocked by the use of condenser apertures shown in Figure 15. Transmitted electrons eventually fall in on a fluorescent screen which can then be researched, in SEM the results can be obtained digitally. Of course not all electrons hit the fluorescent screen, some scatter as well. Figure 14 shows a comparison between both transmission and scanning electron microscopy. The differences in specimen position and detectors is clearly visible here [60], [61], [62].

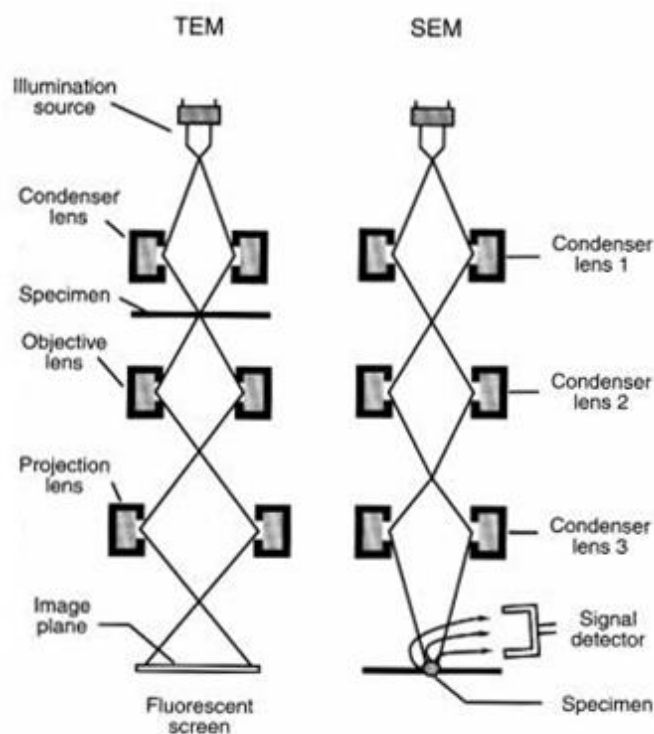


Figure 14. Comparison of TEM and SEM [63]

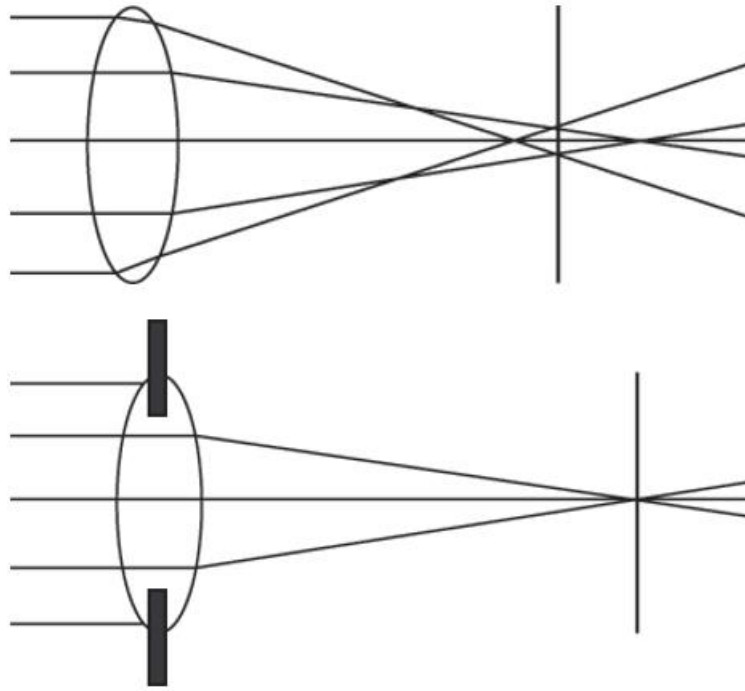


Figure 15. Influence of condenser apertures [63]

TEM operates in vacuum since electrons would deflect off of gas molecules or hydrocarbons, just like SEM. Unlike SEM, sample preparation is different. Because thin slices are required in TEM, necessary steps are preservation, dehydration, cutting, dimpling and staining.

First the sample is placed in a chemical solution to maintain cell structure and then it undergoes dehydration. The sample can now be cut and dimpled. The dimpling procedure creates a thin centre with thicker edges which makes the sample easy to handle. Afterwards it will be stained using a lead solution. This staining procedure provides contrast in the resulting image since it leaves areas dark because electrons cannot pass through the staining chemicals [60], [61], [62], [63].

Because TEM passes through the sample it reveals information on the internal composition, morphology and crystal structure of samples. This makes it useful for different fields such as the industry, medical purposes, semiconductor analysis, nanotechnology... [61], [64].

2.4.3 X-ray diffraction

XRD delivers structural information like crystal size and structure, layer orientation and thickness, and chemical composition in a rapid fashion. It can even provide information on unit cell dimensions and give the fractions of different phases if there were any. For this reason, XRD is used to analyse a broad spectrum of materials, from solids to powders on a nanoscale in which both qualitative and quantitative analysis are possible. Since materials range from solids to powders, minimal sample preparation is required [65], [66].

When monochromatic X-rays penetrate a crystalline sample constructive interference will occur. A cathode ray tube takes on the role of generating these X-rays, which are then filtered to deliver monochromatic radiation and collimated to concentrate before hitting the sample. Incident rays will interact with the specimen and result in constructive interference which

causes a peak in intensity when Bragg's law, illustrated in Figure 16, has been complied with [67].

$$n\lambda = 2d \sin \theta$$

with θ = diffraction angle
 λ = wavelength
 n = an integer
 d = lattice spacing

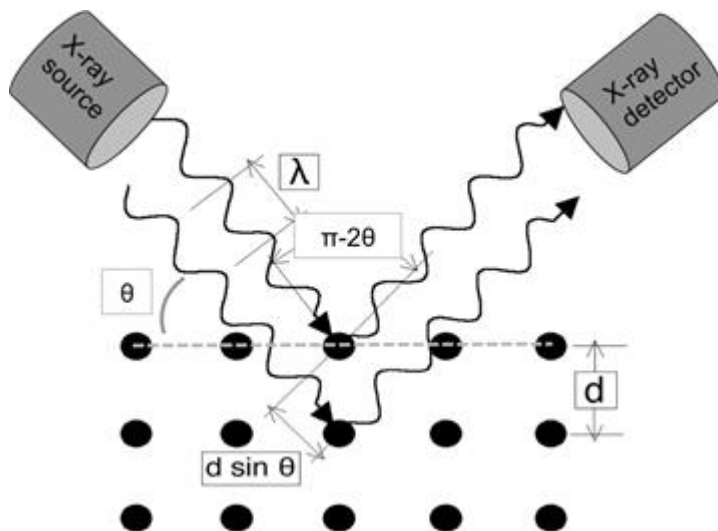


Figure 16. Illustration of Bragg's Law [68]

The rays will then be detected, evaluated and counted. The angle between incident and diffracted rays will be varied over a whole range of values of 2θ to make sure that all diffraction peaks are accounted for. The resulting graph will have ' 2θ ' as its X-axis which typically ranges from $5-70^\circ$ and 'Counts per second' or intensity as its Y-axis as can be seen in Figure 17, and can be cross referenced in a database with reference patterns to identify the chemical composition.

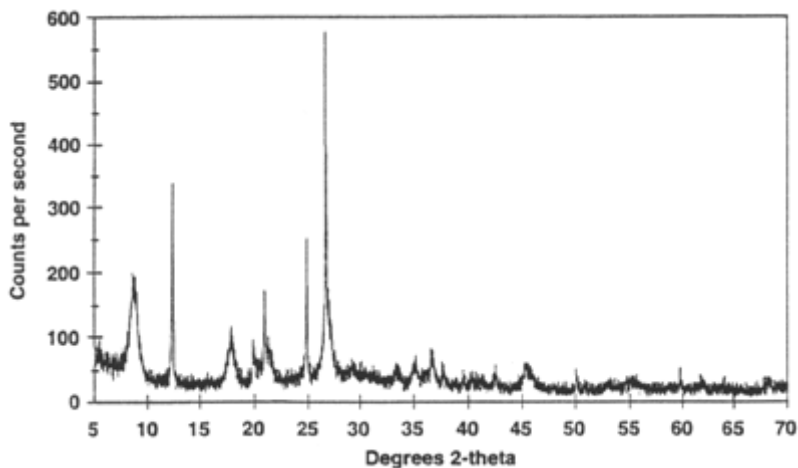


Figure 17. Standard XRD graph [66]

Amorphous parts can be distinguished by broad humps in the intensity and unknowns can be determined since certain sets of lattice spacings are unique for different minerals and deviations from the ideal crystal structure can be obtained resulting from internal stress for example [66], [67], [68].

2.4.4 Energy-Dispersive X-ray spectroscopy

EDX is a chemical micro-analytical method which can be combined with SEM and TEM. As it is carried out in combination with SEM and TEM, samples must meet the same requirements as those for SEM and TEM. It analyses the previously mentioned characteristic X-rays generated from the return of excited electrons to lower energy levels [69], [70], [71], [72]. When electrons at higher energy levels move to vacancies with lower energy levels, elements deliver X-rays with quantities of energy equal to the difference in energy between these higher and lower state of electrons. These higher and lower states differ for every element making X-rays characteristic.

The detector in EDX measures the energy levels of these X-rays and converts it into a voltage pulse. Afterwards the intensity in the form of amount of X-rays is expressed in relation to electron volts [70].

EDX quickly provides information on elementary composition of individual points or line scans. In these line scans, the electron beam follows a pre-programmed line. From this the relative elemental composition can be extracted. This elementary analysis of an individual point can be executed in areas as small as 1 nm. Please note, careful assessment of the spectra is required as peak overlaps of different elements are possible [69].

2.4.5 Photoluminescence

Incoming light will be absorbed by liquids and powders and as a result, electrons will undergo photo-excitation. Since this process starts with the absorption of light, wavelengths will play a part in the resulting spectrum. If interference is an occurring problem, the wavelength should be set properly.

Overtime, these excited electrons will undergo relaxation and energy will be released in the form of fluorescence and phosphorescence as can be seen in Figure 18 below [73], [74], [75].

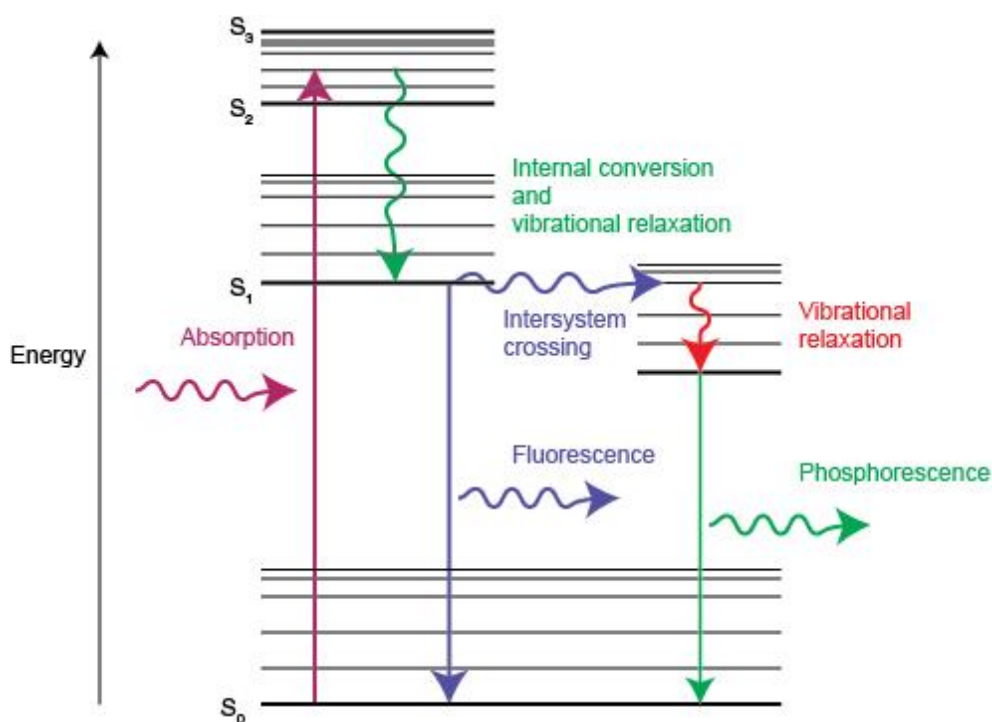


Figure 18. Energy levels of fluorescence and phosphorescence [73]

Transitions such as internal conversion and vibrational relaxation are transitions where no energy is released. The difference between fluorescence and phosphorescence is in the time aspect of relaxation. Relaxation occurs much faster in fluorescence than in phosphorescence. Fluorescence takes place in nanoseconds whereas phosphorescence can take hours or even days [76].

Photoluminescence can be used to determine the band gap which is perfect for this study seeing as there were still some uncertainties about the band gap in the literature. The recombination mechanism will be studied using PL as well. Both the band gap and the recombination mechanism will provide more clarity about the electrical properties. Different wavelengths will be used to achieve absorption, the wavelength that provides the most photoluminescence will also provide the most absorption. This gives an idea about the optical properties of the synthesized catalyst [74].

2.4.6 Fourier-Transform Infrared spectroscopy

If infrared radiation is sent to a sample, parts of this radiation will be absorbed while other parts will pass through the sample. Different wavelengths are absorbed with different intensities by various functional groups related to their vibrational bond energy. After conversion using a Fourier Transform, this forms a characteristic intensity versus frequency spectrum in the mid-infrared region known as a molecular fingerprint. The spectrum of polycarbonate for example, does not look like the spectrum of nylon, whilst all spectra of different forms of nylon will show obvious similarities. Therefore, molecular identification is very fast which makes FTIR a capable method used in chemical and pharmaceutical industries. When FTIR is executed in-situ it gives information about the reaction mechanism, this could prove to be advantageous to get a clear image of the degradation mechanism but this might

not be possible at HUST. Since FTIR can be used as an in-situ method, there is no need for sample preparation. FTIR knows many great applications and that is the reason this analysis will be executed in this research, but results might prove to be useless, seeing as materials, which contain a lot of carbon, absorb a ton of radiation over a great frequency region. This might result in a spectra which lacks the necessary details [77], [78], [79].

3. EXPERIMENTAL

In this part, the foreseen experimental plan will be written out, including the necessary motivation for the activities.

3.1 Synthesis

Before the composite can be synthesized, (r)GO and Fe_3O_4 must be synthesized separately. First the synthesis of GO is performed using an Ultrasonication-assisted modified Hummers' method:

1. 2 g of graphite + 10 ml HNO_3 CONC. and 20 ml H_2SO_4 CONC. (1:2, v/v) in an ice bath ($T < 5^\circ\text{C}$).
2. Slowly add 3 g of KMnO_4 .
3. Heat at 65°C for 2 h in a water bath.
4. Keep under ultrasonication for 2 h to improve the exfoliation of GO.
5. Thoroughly wash the GO using deionized water.
6. Centrifuge and dry at 50°C to obtain GO.

Acquiring rGO requires an extra step on the synthesized GO after the washing step:

1. Reduce the GO by adding hydrazine hydrate (20 mL of 1.0 mM) at pH 10 [80].
2. Keep under ultrasonication for 2 h.
3. Centrifuge and dry at 50°C to obtain rGO.

Next up is the synthesis of Fe_3O_4 according to:

1. 1.7 g $\text{FeCl}_3 \cdot 6\text{H}_2\text{O}$, 1.0 g PEG 6000, and 2.34 g CH_3COONa were dissolved into 40 mL ethylene glycol solution.
2. The mixture was heated at 80°C for 1 h to obtain black precipitates of Fe_3O_4 .
3. The Fe_3O_4 precipitates were collected and cleaned with deionized water and ethanol for four times each followed by drying under vacuum at room temperature for 4 h.

If both (r)GO and Fe_3O_4 are synthesized, $\text{BiOI}/\text{Fe}_3\text{O}_4 @(\text{r})\text{GO}$ can be synthesized:

1. Sonicate the required amount of (r)GO (2,4 and 6 wt%) for 30 min in 100 mL of distilled water .
2. Add 1.0 g $\text{Bi}(\text{NO}_3)_3 \cdot 5\text{H}_2\text{O}$ and 0.50 mg of Fe_3O_4 to the (r)GO solution with magnetic stirring for 10 min.
3. Add 0.37 g KI and 0.35 g CH_3COONa with stirring for 10 min at room temperature followed by ultrasonication for 30 min and aging for 90 min.
4. Separate by using magnets and wash with water and ethanol three times.
5. Dry at 60°C overnight and label as $\text{BiOI}/\text{Fe}_3\text{O}_4 @(\text{r})\text{GO}$.

BiOI/ Fe₃O₄ is also synthesized as a catalyst for comparison, in which case no (r)GO is added. The different weight percentages of the graphene component were chosen based on the work of other researchers as can be seen in

Table 2. If one were to go to higher percentages, irreversible agglomeration would occur as mentioned earlier.

As mentioned in the literature study, the more the structure of the graphene component tends towards pure graphene, the better the catalyst will work. Therefore, it is important to compare catalysts with GO and catalysts with rGO.

There is no expiry date for synthesized samples and in terms of material there is no possibility to perform multiple syntheses in parallel, for these reasons the different components of the synthesis are all performed consecutively.

3.2 Characterization

Characterization is a fast process, this is why it was recommended to perform the synthesis and the characterization + the verification of photocatalytic activity in a consecutive manner. If it turns out that a lot of time is available during the synthesis and some samples are ready for characterisation, these samples will be characterised earlier. This would also be advantageous for the verification step because this requires characterisation before and after degradation.

3.2.1 Theoretical results

In Figure 19 the reference XRD pattern of GO and graphene can be seen, this shows that there are not a lot of peaks. GO has a relatively large peak around $2\theta = 12$ and graphene shows a small hump around $2\theta = 25$. The EDX analysis of $\text{Fe}_3\text{O}_4/\text{BiOI@GO}$ in Figure 20 shows that carbon, bismuth, iron, oxygen and iodine are present. The figures of the PL spectra (Figure 21 and Figure 22) show that we can expect a peak around 500 nm for GO that is concentration dependant. It is also clear that this is not a distinct peak at all since the intensity remains very low compared to the red curve in Figure 21. Finally, in the reference FTIR pattern of GO and graphene (Figure 23) can be seen that GO has more prominent peaks than graphene which was to be expected because there are more interactions in GO because there are more functional groups present such as epoxides and hydroxyl groups. The largest peak of GO can be found at 1087 cm^{-1} and is due to the C-O bonds that are abundantly present.

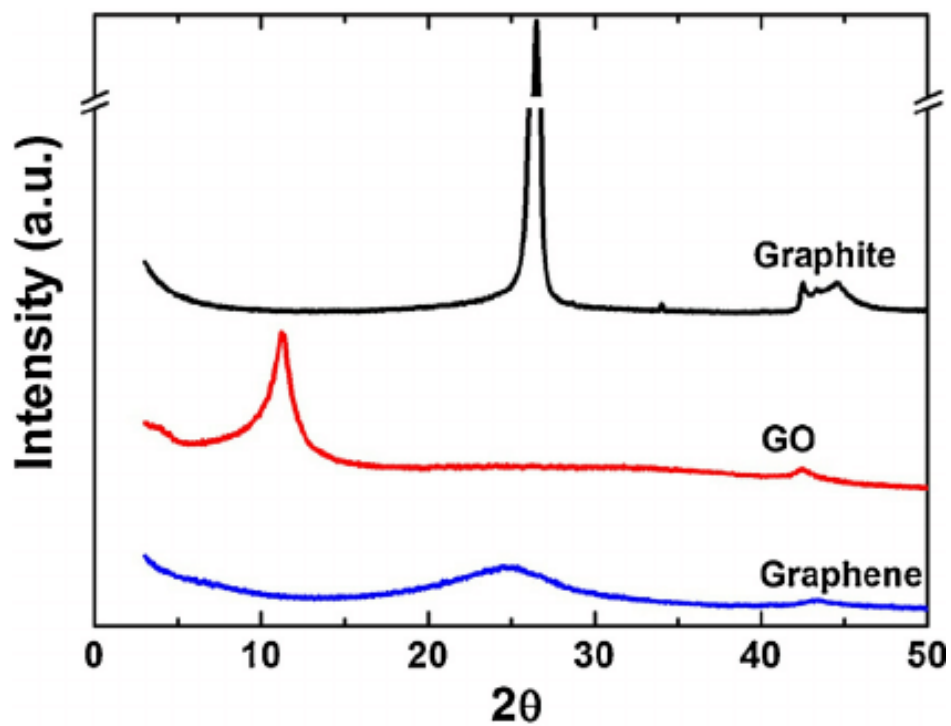


Figure 19. Reference XRD pattern of GO and graphene [81]

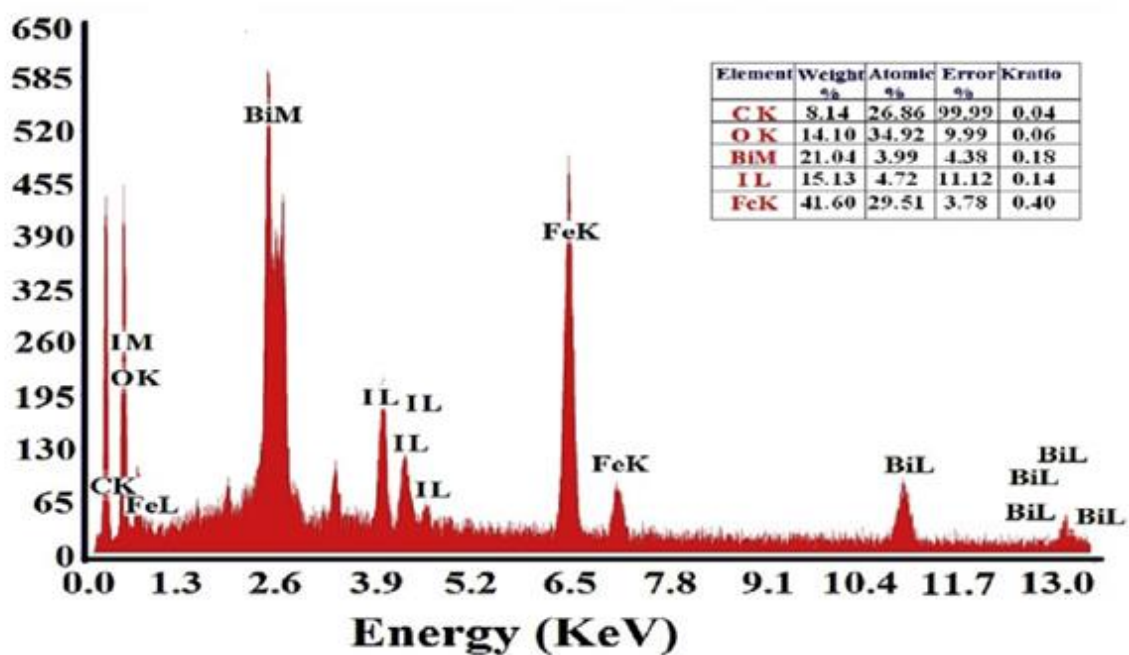


Figure 20. EDX analysis of BiOI/Fe₃O₄@GO [12]

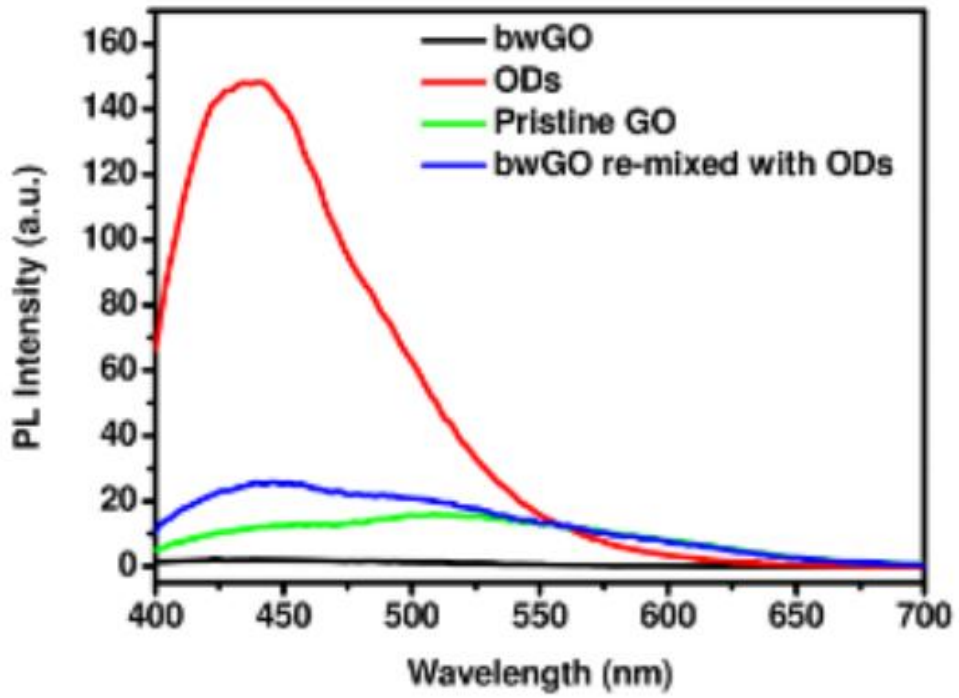


Figure 21. PL spectra of Pristine GO [82]

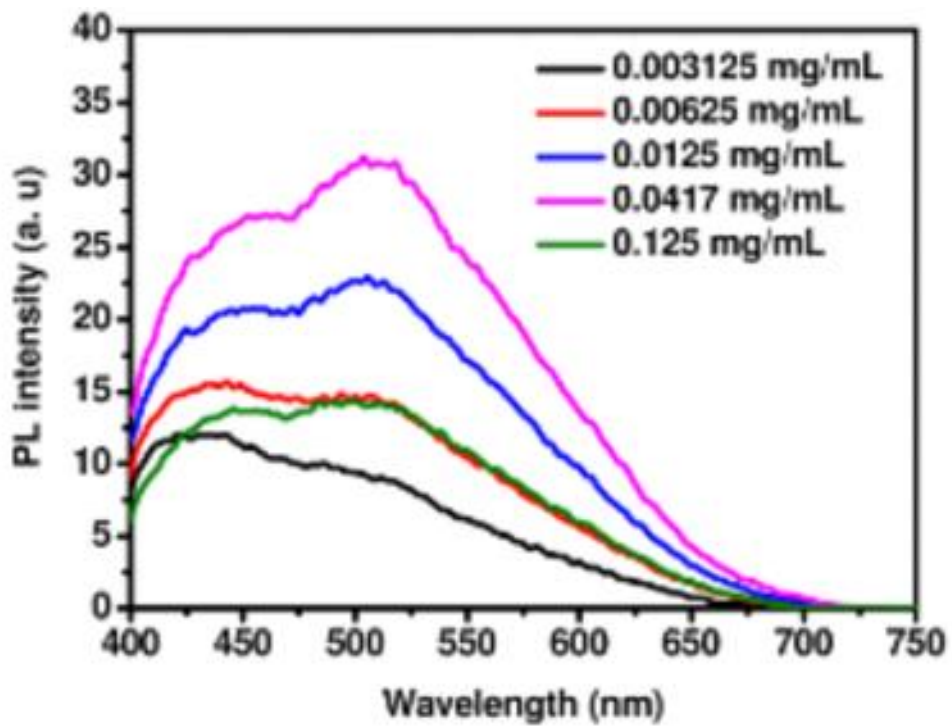


Figure 22. PL spectra of various concentrations of GO at pH = 4 [82]

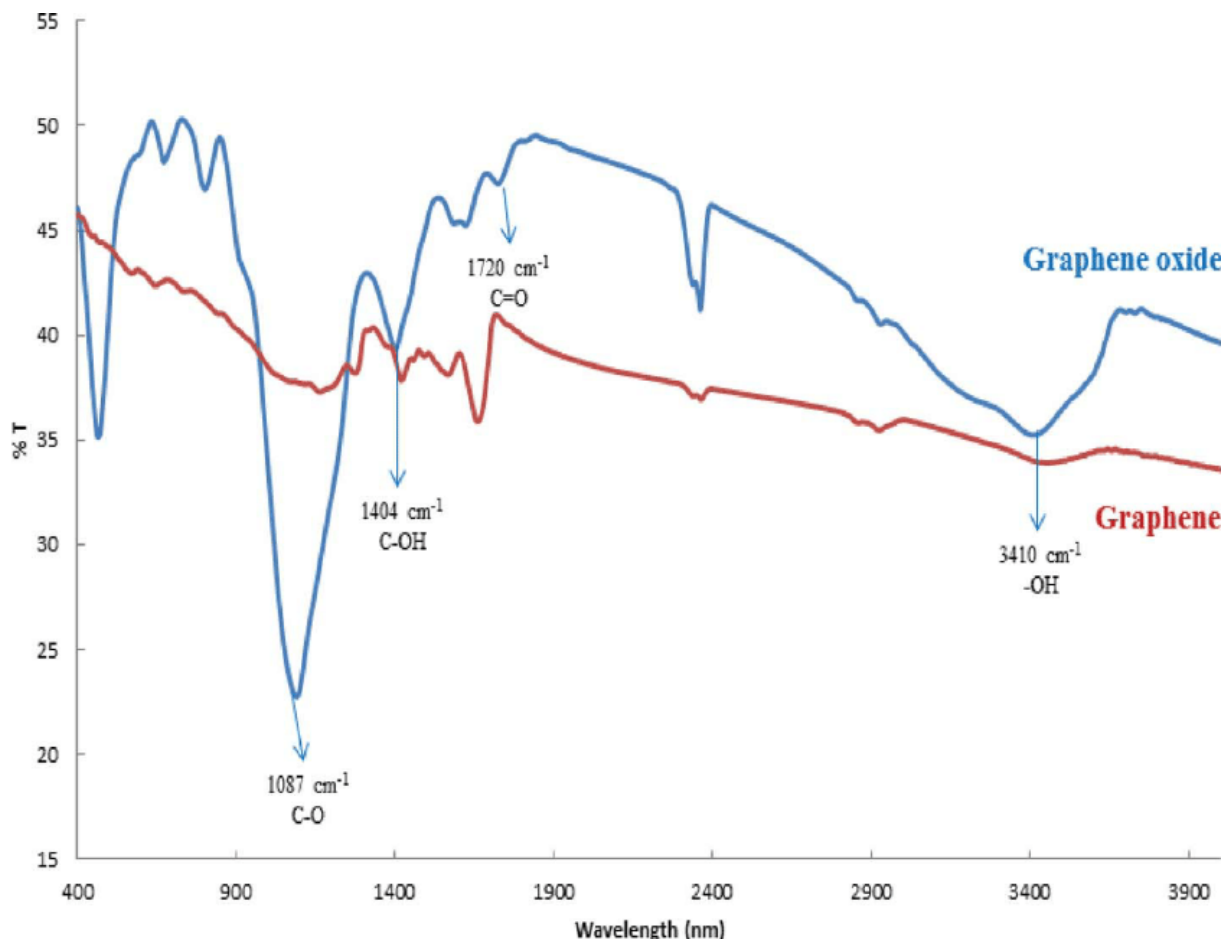


Figure 23. Reference FTIR pattern of graphene and GO [83]

3.3 Verification of the photocatalytic activity

The tests for photocatalytic activity can be carried out at the same time as the characterisation tests. Verification tests must be carried out for different pollutant starting concentrations, with different catalyst loadings and for different catalysts. For BiOI/Fe₃O₄@(r)GO, the reusability will also be tested by performing multiple tests with the same catalyst sample. These tests will be performed with a Xenon or Tungsten lamp of which the wattage must be known, these lamps will simulate visual light.

The starting concentration of the pollutant must always be known and by using the formula below and measuring the transmission/absorption at different times the remaining concentration of the pollutant can be determined at any desired time.

$$E = \left(1 - \frac{C}{C_0}\right) \times 100\% = \left(1 - \frac{A}{A_0}\right) \times 100\%$$

RhB concentrations between 10 - 50 mg/L will be tested, from these results the maximum concentration that can be efficiently degraded should eventually be found. In the study of photocatalytic degradation of antibiotics, the pollutant concentration of 10 mg/L was very

quickly broken down for over 99%. Therefore, higher pollutant concentrations are also investigated in this study.

Catalyst loading is an important factor regarding the degradation rate of the pollutant. The optimal catalyst loading depends on the volume in which the tests are performed and the starting concentration of the pollutant. The optimal catalyst loading from the work of Singh et al. [12] was 0.7 g/L, since the concentration of the pollutant will be varied in this study, the catalyst loading will be varied between 0.5 - 5 g/L catalyst. The explanation for the difference in degradation with different catalyst loadings is that more active sites are present the more catalyst is present. But at a certain moment an optimal concentration is reached. Higher than this optimal concentration, side effects will occur which will even reduce the degradation. Agglomeration and turbidity are side effects. Agglomeration between catalyst particles will reduce the number of active sites and the more catalyst particles are added, the higher the turbidity of the solution. Light will be more difficult to absorb when the solution is more turbid. Testing the reusability by performing multiple tests for photocatalytic activity with the same catalyst sample will be performed as well. This will give an idea of the stability of the catalyst.

REFERENCES

- [1] "HANOI UNIVERSITY OF SCIENCE AND TECHNOLOGY." [Online]. Available: <https://en.hust.edu.vn/web/en/home>.
- [2] "International Training Institute for Materials Science." [Online]. Available: <http://www.itims.edu.vn>.
- [3] F. Chen *et al.*, "Fabrication of Fe₃O₄@SiO₂@TiO₂ nanoparticles supported by graphene oxide sheets for the repeated adsorption and photocatalytic degradation of rhodamine B under UV irradiation," *Dalt. Trans.*, vol. 43, no. 36, pp. 13537–13544, 2014.
- [4] K. Liu, H. Li, Y. Wang, X. Gou, and Y. Duan, "Adsorption and removal of rhodamine B from aqueous solution by tannic acid functionalized graphene," *Colloids Surfaces A Physicochem. Eng. Asp.*, vol. 477, pp. 35–41, 2015.
- [5] E. H. Umukoro, M. G. Peleyeju, J. C. Ngila, and O. A. Arotiba, "Photocatalytic degradation of acid blue 74 in water using Ag-Ag₂O-ZnO nanostructures anchored on graphene oxide," *Solid State Sci.*, vol. 51, pp. 66–73, 2016.
- [6] M. E. Khan, M. M. Khan, and M. H. Cho, "Recent progress of metal-graphene nanostructures in photocatalysis," *Nanoscale*, vol. 10, no. 20, pp. 9427–9440, 2018.
- [7] Y. Wang, L. Guo, P. Qi, X. Liu, and G. Wei, "Synthesis of three-dimensional graphene-based hybrid materials for water purification: A review," *Nanomaterials*, vol. 9, no. 8, 2019.
- [8] W. Zhang, F. Dong, T. Xiong, and Q. Zhang, "Synthesis of BiOBr-graphene and BiOBr-graphene oxide nanocomposites with enhanced visible light photocatalytic performance," *Ceram. Int.*, vol. 40, no. 7 PART A, pp. 9003–9008, 2014.
- [9] V. B. Mohan, K. tak Lau, D. Hui, and D. Bhattacharyya, "Graphene-based materials and their composites: A review on production, applications and product limitations," *Compos. Part B Eng.*, vol. 142, no. December 2017, pp. 200–220, 2018.
- [10] K. Zhu *et al.*, "Graphene covered SiC powder as advanced photocatalytic material," *Appl. Phys. Lett.*, vol. 100, no. 2, 2012.
- [11] H. Brody, P. Murphy, and Y. Smith, "Nature Outlook Graphene," p. 70, 2012.
- [12] P. Singh, A. Sudhaik, P. Raizada, P. Shandilya, R. Sharma, and A. Hosseini-Bandegharai, "Photocatalytic performance and quick recovery of BiOI/Fe₃O₄@graphene oxide ternary photocatalyst for photodegradation of 2,4-dinitrophenol under visible light," *Mater. Today Chem.*, vol. 12, pp. 85–95, 2019.
- [13] R. Vinoth, S. G. Babu, R. Ramachandran, and B. Neppolian, "Bismuth oxyiodide incorporated reduced graphene oxide nanocomposite material as an efficient photocatalyst for visible light assisted degradation of organic pollutants," *Appl. Surf. Sci.*, vol. 418, pp. 163–170, 2017.
- [14] M. J. F. Calvete, G. Piccirillo, C. S. Vinagreiro, and M. M. Pereira, "Hybrid materials for heterogeneous photocatalytic degradation of antibiotics," *Coord. Chem. Rev.*, vol. 395, pp. 63–85, 2019.
- [15] M. Arumugam and M. Y. Choi, "Recent progress on bismuth oxyiodide (BiOI) photocatalyst for environmental remediation," *J. Ind. Eng. Chem.*, vol. 81, pp. 237–268, 2020.
- [16] C. Hui *et al.*, "Large-scale Fe₃O₄ nanoparticles soluble in water synthesized by a facile method," *J. Phys. Chem. C*, vol. 112, no. 30, pp. 11336–11339, 2008.
- [17] C. Wang *et al.*, "Photocatalytic degradation of bisphenol A and dye by graphene-oxide/Ag₃PO₄ composite under visible light irradiation," *Ceram. Int.*, vol. 40, no. 6, pp. 8061–8070, 2014.
- [18] R. Nagaraja, N. Kottam, C. R. Girija, and B. M. Nagabhushana, "Photocatalytic

- degradation of Rhodamine B dye under UV/solar light using ZnO nanopowder synthesized by solution combustion route," *Powder Technol.*, vol. 215–216, pp. 91–97, 2012.
- [19] G. M. Neelgund, A. Oki, and Z. Luo, "ZnO and cobalt phthalocyanine hybridized graphene: Efficient photocatalysts for degradation of rhodamine B," *J. Colloid Interface Sci.*, vol. 430, pp. 257–264, 2014.
- [20] C. J. Miller, H. Yu, and T. D. Waite, "Degradation of rhodamine B during visible light photocatalysis employing Ag@AgCl embedded on reduced graphene oxide," *Colloids Surfaces A Physicochem. Eng. Asp.*, vol. 435, pp. 147–153, 2013.
- [21] S. Guo, G. Zhang, and J. C. Yu, "Enhanced photo-Fenton degradation of rhodamine B using graphene oxide-amorphous FePO₄ as effective and stable heterogeneous catalyst," *J. Colloid Interface Sci.*, vol. 448, pp. 460–466, 2015.
- [22] "Triarylmethane_dye @ en.wikipedia.org." [Online]. Available: https://en.wikipedia.org/wiki/Triarylmethane_dye.
- [23] "Rhodamine @ en.wikipedia.org." [Online]. Available: <https://en.wikipedia.org/wiki/Rhodamine>.
- [24] "rhodamine @ www.merriam-webster.com." [Online]. Available: <https://www.merriam-webster.com/dictionary/rhodamine>.
- [25] "Rhodamine-B @ Www.Sigmaaldrich.Com." [Online]. Available: <http://www.sigmaaldrich.com/catalog/search?term=90-12-0&interface=CASNo.&N=0&mode=partialmax&lang=en®ion=US&focus=product>.
- [26] "Rhodamine-B @ www.sciencedirect.com." [Online]. Available: <https://www.sciencedirect.com/topics/chemistry/rhodamine-b>.
- [27] "The-history-of-graphene @ graphene-flagship.eu." [Online]. Available: <https://graphene-flagship.eu/material/Pages/The-history-of-graphene.aspx>.
- [28] X. Liu, *Nanomechanics of Graphene and Design of Graphene Composites*. 2019.
- [29] C. Verma and E. E. Ebenso, "Ionic liquid-mediated functionalization of graphene-based materials for versatile applications: a review," *Graphene Technol.*, vol. 4, no. 1–2, pp. 1–15, 2019.
- [30] G. Gonçalves, P. Marques, and M. Vila, *Carbon Nanostructures Graphene-based Materials in Health and Environment New Paradigms*. 2016.
- [31] "two-dimensional-dirac-materials-properties-rarity @ phys.org," 04/2015. [Online]. Available: <https://phys.org/news/2015-04-two-dimensional-dirac-materials-properties-rarity.html>.
- [32] B. G. Kim and H. J. Choi, "Graphyne: Hexagonal network of carbon with versatile Dirac cones," *Phys. Rev. B - Condens. Matter Mater. Phys.*, vol. 86, no. 11, pp. 1–5, 2012.
- [33] W. S. Hummers and J. R. E. Offeman, "Preparation of Graphitic Oxide," *J. Am. Chem. Soc.*, vol. 80, no. 6, pp. 1339–1339, 1958.
- [34] S. Sahoo, S. K. Tiwari, and G. C. Nayak, *Surface Engineering of Graphene*. 2019.
- [35] P. Shandilya *et al.*, "Fabrication of fluorine doped graphene and SmVO₄ based dispersed and adsorptive photocatalyst for abatement of phenolic compounds from water and bacterial disinfection," *J. Clean. Prod.*, vol. 203, pp. 386–399, 2018.
- [36] Z. Liu *et al.*, "Decoration of BiOI quantum size nanoparticles with reduced graphene oxide in enhanced visible-light-driven photocatalytic studies," *Appl. Surf. Sci.*, vol. 259, pp. 441–447, 2012.
- [37] "photocatalysts @ www.sciencedirect.com." [Online]. Available: <https://www.sciencedirect.com/topics/engineering/photocatalysts>.
- [38] J. Zhang, B. Tian, L. Wang, M. Xing, and J. Lei, *Mechanism of Photocatalysis*. 2018.
- [39] S. M. Rodríguez, J. Blanco Gálvez, and C. A. Estrada Gasca, "Photocatalysis," *Sol. Energy*,

- vol. 77, no. 5, pp. 443–444, 2004.
- [40] S. Zhu and D. Wang, “Photocatalysis: Basic principles, diverse forms of implementations and emerging scientific opportunities,” *Adv. Energy Mater.*, vol. 7, no. 23, pp. 1–24, 2017.
- [41] X. Li, Q. Wang, Y. Zhao, W. Wu, J. Chen, and H. Meng, “Green synthesis and photocatalytic performances for ZnO-reduced graphene oxide nanocomposites,” *J. Colloid Interface Sci.*, vol. 411, pp. 69–75, 2013.
- [42] D. Chatterjee and S. Dasgupta, “Visible light induced photocatalytic degradation of organic pollutants,” *J. Photochem. Photobiol. C Photochem. Rev.*, vol. 6, no. 2–3, pp. 186–205, 2005.
- [43] M. M. Khan, S. F. Adil, and A. Al-Mayouf, “Metal oxides as photocatalysts,” *J. Saudi Chem. Soc.*, vol. 19, no. 5, pp. 462–464, 2015.
- [44] I *et al.*, “Typical non-TiO₂-based visible-light photocatalysts,” *Intech*, vol. i, no. tourism, p. 13, 2012.
- [45] M. Meksi, A. Turki, H. Kochkar, L. Bousselmi, C. Guillard, and G. Berhault, “The role of lanthanum in the enhancement of photocatalytic properties of TiO₂ nanomaterials obtained by calcination of hydrogenotitanate nanotubes,” *Appl. Catal. B Environ.*, vol. 181, pp. 651–660, 2016.
- [46] A. Khataee, R. D. C. Soltani, Y. Hanifehpour, M. Safarpour, H. Gholipour Ranjbar, and S. W. Joo, “Synthesis and characterization of dysprosium-doped ZnO nanoparticles for photocatalysis of a textile dye under visible light irradiation,” *Ind. Eng. Chem. Res.*, vol. 53, no. 5, pp. 1924–1932, 2014.
- [47] B. Weng, M. Y. Qi, C. Han, Z. R. Tang, and Y. J. Xu, “Photocorrosion Inhibition of Semiconductor-Based Photocatalysts: Basic Principle, Current Development, and Future Perspective,” *ACS Catal.*, vol. 9, no. 5, pp. 4642–4687, 2019.
- [48] D. S. Bhachu *et al.*, “Bismuth oxyhalides: Synthesis, structure and photoelectrochemical activity,” *Chem. Sci.*, vol. 7, no. 8, pp. 4832–4841, 2016.
- [49] M. Arumugam and M. Y. Choi, “Recent progress on bismuth oxyiodide (BiOI) photocatalyst for environmental remediation,” *J. Ind. Eng. Chem.*, vol. 81, pp. 237–268, 2020.
- [50] “DIRECT BAND GAP AND INDIRECT BAND GAP SEMICONDUCTORS.” [Online]. Available: <https://www.upscgetway.com/direct-band-gap-and-indirect-band-gap-semiconductors/>.
- [51] E. Kowsari, *Carbon-Based Nanocomposites for Visible Light-Induced Photocatalysis*. 2017.
- [52] L. Zhang and M. Jaroniec, “Toward designing semiconductor-semiconductor heterojunctions for photocatalytic applications,” *Appl. Surf. Sci.*, vol. 430, pp. 2–17, 2018.
- [53] M. P. Mikhailova, K. D. Moiseev, and P. Y. Yakovlev, “Interface-induced optical and transport phenomena in type II broken-gap single heterojunctions,” *Semicond. Sci. Technol.*, vol. 19, no. 10, 2004.
- [54] C. Guo, S. Gao, J. Lv, S. Hou, Y. Zhang, and J. Xu, “Assessing the photocatalytic transformation of norfloxacin by BiOBr/iron oxides hybrid photocatalyst: Kinetics, intermediates, and influencing factors,” *Appl. Catal. B Environ.*, vol. 205, pp. 68–77, 2017.
- [55] C. Guo *et al.*, “Novel magnetically recoverable BiOBr/iron oxides heterojunction with enhanced visible light-driven photocatalytic activity,” *Appl. Surf. Sci.*, vol. 320, pp. 383–390, 2014.
- [56] “SEM @ serc.carleton.edu.” [Online]. Available:

- http://serc.carleton.edu/research_education/geochemsheets/techniques/SEM.html.
- [57] "Scanning Electron Microscopy @ www.nanoscience.com." [Online]. Available: <https://www.nanoscience.com/techniques/scanning-electron-microscopy/>.
- [58] B. D. Fahlman, "Materials Characterization @ link.springer.com," 2018. [Online]. Available: https://link.springer.com/chapter/10.1007/978-94-024-1255-0_7.
- [59] R. F. Egerton, "Physical principles of electron microscopy: An introduction to TEM, SEM, and AEM, second edition," *Phys. Princ. Electron Microsc. An Introd. to TEM, SEM, AEM, Second Ed.*, pp. 1–196, 2016.
- [60] University of California, "Transmission-Electron-Microscope @ [Www.Ccber.Ucsb.Edu](http://www.ccber.ucsb.edu)." [Online]. Available: <https://www.ccber.ucsb.edu/collections-botanical-collections-plant-anatomy/transmission-electron-microscope>. [Accessed: 14-Apr-2020].
- [61] R. Rajan, "Difference_between_SEM_and_TEM_techniques2 @ www.researchgate.net." [Online]. Available: https://www.researchgate.net/post/What_is_the_difference_between_SEM_and_TEM_techniques2.
- [62] Physics, "Transmission Electron Microscopy (TEM) @ warwick.ac.uk." [Online]. Available: <https://warwick.ac.uk/fac/sci/physics/current/postgraduate/regs/mpagswarwick/ex5/techniques/structural/tem/>. [Accessed: 14-Apr-2020].
- [63] The University of Iowa (TEM), "Transmission-Electron-Microscopy @ [Cmrf.Research.Uiowa.Edu](http://cmrf.research.uiowa.edu)." [Online]. Available: <https://cmrf.research.uiowa.edu/transmission-electron-microscopy>. [Accessed: 14-Apr-2020].
- [64] TEM2, "Transmission-Electron-Microscope @ [Www.Microscopemaster.Com](http://www.microscopemaster.com)." [Online]. Available: <https://www.microscopemaster.com/transmission-electron-microscope.html>. [Accessed: 14-Apr-2020].
- [65] Malvern Panalytical, "x-ray-diffraction @ www.malvernpanalytical.com." [Online]. Available: <https://www.malvernpanalytical.com/en/products/technology/x-ray-diffraction>. [Accessed: 14-Apr-2020].
- [66] B. L. D. and C. M. Clark, "XRD @ serc.carleton.edu," *Lsf*. [Online]. Available: http://serc.carleton.edu/research_education/geochemsheets/techniques/XRD.html. [Accessed: 14-Apr-2020].
- [67] XOS, "XRD @ www.xos.com," 2020. [Online]. Available: <https://www.xos.com/XRD>. [Accessed: 14-Apr-2020].
- [68] "x-ray-diffraction @ www.jove.com." [Online]. Available: <https://www.jove.com/science-education/10446/x-ray-diffraction>. [Accessed: 14-Apr-2020].
- [69] EAG Laboratories, "Energy Dispersive Spectroscopy (EDS) @ www.eag.com." [Online]. Available: <https://www.eag.com/nl/techniques/spectroscopy/energy-dispersive-x-ray-spectroscopy-eds/>. [Accessed: 14-Apr-2020].
- [70] Materials evaluation and engineering, "ENERGY DISPERSIVE X-RAY SPECTROSCOPY (EDS) @ www.mee-inc.com," 2019. [Online]. Available: <https://www.mee-inc.com/hamm/energy-dispersive-x-ray-spectroscopyeds/>. [Accessed: 14-Apr-2020].
- [71] Clean Energy Institute, "Energy Dispersive X-ray Spectroscopy @ www.cei.washington.edu," 2020. [Online]. Available: <https://www.cei.washington.edu/education/science-of-solar/energy-dispersive-x-ray-spectroscopy/>. [Accessed: 14-Apr-2020].
- [72] "energy-dispersive-x-ray-spectroscopy @ www.sciencedirect.com." [Online]. Available: <https://www.sciencedirect.com/topics/engineering/energy-dispersive-x-ray>

- spectroscopy. [Accessed: 14-Apr-2020].
- [73] Renishaw, “photoluminescence-explained--25809 @ www.renishaw.nl.” [Online]. Available: <https://www.renishaw.nl/nl/photoluminescence-explained--25809>. [Accessed: 14-Apr-2020].
- [74] Horiba, “Photoluminescence (PL) & Electroluminescence (EL) @ www.horiba.com.” [Online]. Available: https://www.horiba.com/en_en/products/by-technique/molecular-spectroscopy/photoluminescence-pl-electroluminescence-el/. [Accessed: 14-Apr-2020].
- [75] M. Goswami and A. K. Meikap, “photoluminescence @ www.sciencedirect.com.” [Online]. Available: <https://www.sciencedirect.com/topics/materials-science/photoluminescence>.
- [76] Princeton Instruments, “fluorescence-phosphorescence-photoluminescence @ www.princetoninstruments.com.” [Online]. Available: <https://www.princetoninstruments.com/applications/fluorescence-phosphorescence-photoluminescence>. [Accessed: 14-Apr-2020].
- [77] Mettler Toledo, “ftir-spectroscopy @ www.mt.com.” [Online]. Available: https://www.mt.com/int/en/home/products/L1_AutochemProducts/ReactIR/ftir-spectroscopy.html?cmp=sea_01010123&SE=GOOGLE&Campaign=MT_AC_EN_ROW&Adgroup=In+Situ+Analysis+-+FTIR+-+Broad&bookedkeyword=ftir&matchtype=e&adtext=264382117341&placement=&network=g&kcl. [Accessed: 14-Apr-2020].
- [78] Intertek, “Fourier Transform Infrared Spectrometry (FTIR) @ www.intertek.nl.” [Online]. Available: <http://www.intertek.nl/laboratorium/IR-analyse/>. [Accessed: 14-Apr-2020].
- [79] M. Bradley, “Ftir-Basics @ Www.Thermofisher.Com.” [Online]. Available: <https://www.thermofisher.com/es/es/home/industrial/spectroscopy-elemental-isotope-analysis/spectroscopy-elemental-isotope-analysis-learning-center/molecular-spectroscopy-information/ftir-information/ftir-basics.html#>. [Accessed: 14-Apr-2020].
- [80] S. A. Bakar *et al.*, “Improved DSSC photovoltaic performance using reduced graphene oxide–carbon nanotube/platinum assisted with customised triple-tail surfactant as counter electrode and zinc oxide nanowire/titanium dioxide nanoparticle bilayer nanocomposite as photoanode,” *Graphene Technol.*, vol. 4, no. 1–2, pp. 17–31, 2019.
- [81] “XRD-patterns-of-graphite-graphene-oxide-and-graphene_fig1_263509024 @ www.researchgate.net.” [Online]. Available: https://www.researchgate.net/figure/XRD-patterns-of-graphite-graphene-oxide-and-graphene_fig1_263509024.
- [82] D. Du, H. Song, Y. Nie, X. Sun, L. Chen, and J. Ouyang, “Photoluminescence of Graphene Oxide in Visible Range Arising from Excimer Formation,” *J. Phys. Chem. C*, vol. 119, no. 34, pp. 20085–20090, 2015.
- [83] “FTIR-spectrum-of-graphene-oxide-and-graphene_fig1_271672218 @ www.researchgate.net.” [Online]. Available: https://www.researchgate.net/figure/FTIR-spectrum-of-graphene-oxide-and-graphene_fig1_271672218.